# Differentiation signals from glia are fine-tuned to set neuronal numbers during development

Anadika R. Prasad[1], Inês Lago-Baldaia[1], Matthew P. Bostock[1], Zaynab Housseini[1] and Vilaiwan M. Fernandes[1]*.

[1]Department of Cell and Developmental Biology, University College London, Gower Street, London, WC1E 6DE.

*Corresponding author; vilaiwan.fernandes@ucl.ac.uk

**Summary:** Neural circuit formation and function require that diverse neurons are specified in appropriate numbers. Known strategies for controlling neuronal numbers involve regulating either cell proliferation or survival. We used the *Drosophila* visual system to probe how neuronal numbers are set. Photoreceptors from the eye-disc induce their target field, the lamina, such that for every unit eye there is a corresponding lamina unit (column). Although each column initially contains ~6 post-mitotic lamina precursors, only 5 differentiate into neurons, called L1-L5; the 'extra' precursor, which is invariantly positioned above the L5 neuron in each column, undergoes apoptosis. Here, we showed that a glial population called the outer chiasm giant glia ($xg^O$), which resides below the lamina, secretes multiple ligands to induce L5 differentiation in response to EGF from photoreceptors. By forcing neuronal differentiation in the lamina, we uncovered that though fated to die, the 'extra' precursor is specified as an L5. Therefore, two precursors are specified as L5s but only one differentiates during normal development. We found that the row of precursors nearest to $xg^O$ differentiate into L5s and, in turn, antagonise differentiation signalling to prevent the 'extra' precursors from differentiating, resulting in their death. Thus, an intricate interplay of glial signals and feedback from differentiating neurons defines an invariant and stereotyped pattern of neuronal differentiation and programmed cell death to ensure that lamina columns each contain exactly one L5 neuron.

**Keywords:** Neuronal numbers, Glia, *Drosophila* visual system, Neuronal differentiation, Programmed cell death

## Introduction

Many sensory systems consist of repeated circuit units that map stimuli from the outside world onto sequential processing layers (Luo and Flanagan, 2007). It is critical that both absolute and relative neuronal numbers are carefully controlled for these circuits to assemble with topographic correspondence across processing layers. Neuronal numbers can be set by controlling how many progeny a neural stem cell produces, or by regulating how many neural progeny survive (Hidalgo, 2003; Miguel-Aliaga and Thor, 2009). To investigate other developmental strategies that set neuronal numbers, we used the highly ordered and repetitive *Drosophila melanogaster* visual system. Like vertebrate visual systems, the fly visual system is organized retinotopically into repeated modular circuits that process sensory input from unique points in space spanning the entire visual field (Hadjieconomou et al., 2011; Malin and Desplan, 2021).

Retinotopy between the compound eye and the first neuropil in the optic lobe, the lamina, is built during development. Photoreceptors are born progressively in the eye imaginal disc as a wave of differentiation sweeps across the tissue from posterior to anterior. Newly born photoreceptors express Hedgehog (Hh), which promotes further wave propagation (Treisman, 2013). They also express the Epidermal Growth Factor (EGF), Spitz (Spi), which recruits additional photoreceptors into developing ommatidia (Treisman, 2013). As photoreceptors are born, their axons project into the optic lobe and induce the lamina, such that there is a corresponding lamina unit (or cartridge) for every ommatidium (Figure 1A) (Hadjieconomou et al., 2011). Each cartridge is composed of five interneurons (L1-L5; named for the medulla layers they project to) and multiple glial subtypes (Fischbach and Dittrich, 1989; Hadjieconomou et al., 2011).

Lamina induction is a multi-step process triggered by photoreceptor-derived signals. Photoreceptor-derived Hh converts neuroepithelial cells into lamina precursor cells (LPCs), promotes their terminal divisions and drives the assembly of lamina pre-cartridges referred to as columns, *i.e.* ensembles of ~6 post-mitotic LPCs stacked together and associated with photoreceptor axon bundles (Figure 1A,B) (Huang and Kunes, 1998, 1996; Sugie et al., 2010; Umetsu et al., 2006). Once assembled into columns, LPCs are diversified by graded Hh signalling along the distal-proximal axis of young columns (Bostock et al., 2022). They then differentiate into neurons following an invariant spatio-temporal pattern whereby the most

61 proximal (bottom) and most distal (top) cells differentiate first into L5 and L2, respectively;
62 differentiation then proceeds in a distal-to-proximal (top-to-bottom) sequence, L3 forming next,
63 followed by L1, then L4 (Fernandes et al., 2017; Huang et al., 1998; Tan et al., 2015). The sixth
64 LPC, located between L4 and L5, does not differentiate but instead is fated to die by apoptosis
65 and is later cleared (Figure 1A) (Apitz and Salecker, 2014). This spatio-temporal pattern of
66 neuronal differentiation is driven in part by a population of glia called wrapping glia, which
67 ensheathes photoreceptor axons and which induces L1-L4 neuronal differentiation via Insulin/
68 Insulin-like growth factor signalling in response to EGF from photoreceptors (Fernandes et al.,
69 2017). Intriguingly, L1-L4 neuronal differentiation can be disrupted by manipulating wrapping
70 glia without affecting L5 differentiation (Fernandes et al., 2017). Indeed, the mechanisms that
71 drive L5 differentiation are not known. Importantly, we do not understand how exactly 5 neuron
72 types differentiate from 6 LPCs; in other words, how are lamina neuronal numbers set?
73 Here, we sought to determine the mechanisms that drive L5 differentiation as well as
74 those that set neuronal numbers in the lamina. We found that a population of glia located
75 proximal to the lamina, called the outer chiasm giant glia ($xg^O$), induces L5 neuronal
76 differentiation in response to EGF from photoreceptors. We showed that the $xg^O$ secrete multiple
77 signals, including the EGF Spi and a type IV collagen, Collagen type IV alpha 1 (Col4a1), which
78 activate Mitogen-Activated Protein Kinase (MAPK) signalling in the most proximal row of
79 LPCs (*i.e.,* the row of LPCs nearest to $xg^O$), thus driving their differentiation into L5s and
80 promoting their survival. Further, we found that the 'extra' LPCs normally fated to die are
81 specified with L5, but not L1-L4, identity. Since the most proximal row of LPCs are in closest
82 proximity to the $xg^O$, they receive differentiation cues from $xg^O$ first and differentiate into L5s.
83 In turn, these newly induced L5s secrete high levels of Argos (Aos), an antagonist of Spi
84 (Freeman et al., 1992), to limit MAPK activity in the 'extra' LPCs thus preventing their
85 differentiation, and leading to their death and clearance. Thus, we highlight a new mode by
86 which neuronal numbers can be set – not only by regulating the number of neurons born or the
87 number that survive, but also by regulating the number induced to differentiate from a larger
88 pool of precursors. Altogether, our results indicate that the sterotyped pattern of neuronal
89 differentiation and programmed cell death in the lamina are determined by the architecture of the
90 developing tissue together with feedback from newly differentiating neurons.
91

92 **Results**

93 *L5 neuronal differentiation requires EGF Receptor activity in outer chiasm giant glia ($xg^O$)*

94 We showed previously that wrapping glia induce L1-L4 neuronal differentiation in
95 response to EGF from photoreceptors, but that L5 differentiation was regulated independently by
96 an unknown mechanism (Fernandes et al., 2017). We speculated that another glial population
97 may be involved in inducing L5 differentiation in response to EGF from photoreceptors. To test
98 this hypothesis, we blocked EGF Receptor signalling in all glia using a pan-glial driver to
99 express a dominant negative form of EGFR *(Repo>$EGFR^{DN}$)*. Although LPCs (Dac+ cells) still
100 formed and assembled into columns, there was a complete block in lamina neuron differentiation
101 as seen by the absence of the pan-neuronal marker, Embryonic lethal abnormal vision (Elav);
102 *i.e.,* L5 differentiation was disrupted in addition to the differentiation of L1-L4 as expected
103 (Figure 1C, D). Thus, EGFR activity in a glial population other than the wrapping glia is
104 required for L5 neuronal differentiation.

105 Many glial types infiltrate the lamina (Figure1 - Figure Supplement 1A) (Chotard and
106 Salecker, 2007; Edwards et al., 2012). Therefore, we performed a screen using glia subtype-
107 specific Gal4s to block EGFR signalling and determined what effect this manipulation had on
108 L5s using Elav expression in the proximal lamina (Figure1 - Figure Supplement 1B-M;
109 summarised in Supporting File 1). Blocking EGFR signalling in the outer chiasm giant glia ($xg^O$)
110 led to a dramatic reduction in the number of L5s (Figure 1E,F). To rule out early developmental
111 defects, we used a temperature sensitive Gal80 ($Gal80^{ts}$) and shifted animals from the permissive
112 temperature to the restrictive temperature to limit $EGFR^{DN}$ expression in $xg^O$ to begin from the
113 3rd larval instar, when lamina development initiates. This resulted in a similar loss of Elav-
114 positive cells in the proximal lamina as when $EGFR^{DN}$ was expressed continuously in the $xg^O$,
115 indicating that this phenotype is not due to an early defect in $xg^O$ (Figure 1 - Figure Supplement
116 1N). $Xg^O$ are located below the lamina plexus, often with just one or two glial cells spanning the
117 entire width of the lamina. While $xg^O$ extend fine processes towards the lamina, they do not
118 appear to contact LPCs or L5 neurons (Figure 1 - Figure Supplement 1O). Importantly, blocking
119 EGFR signalling in the $xg^O$ did not affect $xg^O$ numbers or morphology (Figure 1E,F, Figure 1 -
120 Figure Supplement 1O-R).

121 Since our screen used Elav expression in the proximal lamina to assess for the presence
122 of L5s, we next examined lamina neuron type markers to assess whether blocking EGFR activity

123 in $xg^O$ affected L5 neurons specifically. We used antibodies against Sloppy paired 2 (Slp2),
124 Brain-specific homeobox (Bsh) and Seven-up (Svp) in combination to distinguish lamina neuron
125 types: L2s and L3s express Slp2 alone, L1s co-express Svp and Slp2, L4s express Bsh alone and
126 L5s co-express Bsh and Slp2 (Figure 1G) (Fernandes et al., 2017; Hasegawa et al., 2013; Tan et
127 al., 2015). We found that the number of L5 neurons decreased specifically, while the number of
128 all the other neuron types were unaffected (Figure 1G-I; $P^{L5}<0.0001$, Mann-Whitney U-test).
129 Finally, to test whether the absence of L5s simply reflected a developmental delay in
130 differentiation, we examined adult optic lobes using a different L5 neuronal marker, POU
131 domain motif 3 (Pdm3) (Tan et al., 2015). Similar to our results in the developing lamina, L5s
132 were mostly absent in the adult lamina when EGFR was blocked in $xg^O$ compared with controls
133 (Figure 1- Figure Supplement 1S,T; $N^{exp}=10$; $N^{ctrl}=11$), indicating that the loss of L5s observed
134 during development is not due to delayed induction. Thus, EGFR activity in $xg^O$ is required for
135 L5 neuronal differentiation.
136
137 *LPCs that fail to differentiate as L5s are eliminated by apoptosis*
138 The loss of L5 neurons when EGFR was blocked in $xg^O$ could be explained either by a
139 defect in neuronal differentiation, or by an earlier defect in LPC formation or recruitment to
140 columns. To distinguish between these possibilities, we counted the number of LPCs per column
141 when EGFR signalling was blocked in $xg^O$ compared to controls (Figure 2A-C). For these and
142 later analyses we considered the youngest column located adjacent to the lamina furrow to be the
143 first column, with column number (and age) increasing towards the posterior side (Figure 1A). In
144 columns 1-4, there were no differences in the number of LPCs when EGFR was blocked in $xg^O$,
145 indicating that LPC formation and column assembly occurred normally (Figure 2C), supporting
146 the hypothesis that in response to EGFR activity, $xg^O$ induce proximal LPCs to differentiate as
147 L5s. Interestingly, the number of LPCs began to decrease in older columns (column 5 onwards)
148 when EGFR signalling was blocked in $xg^O$ (Figure 2C; $P^*<0.05$, $P^{****}<0.0002$, Mann-Whitney
149 U-Test). This observation suggested that undifferentiated LPCs in older columns were being
150 eliminated. We wondered whether LPCs that failed to differentiate into L5s underwent apoptosis,
151 similar to the 'extra' LPCs that undergo apoptosis in controls. We used an antibody against the
152 cleaved form of Death Caspase-1 (Dcp-1), an effector caspase, to detect apoptotic cells
153 (Akagawa et al., 2015) and, indeed, observed a significant increase in the number of Dcp-1

154 positive cells in the lamina when EGFR signalling was blocked in the $xg^O$ (132.8 cells/unit
155 volume ± 19.48 standard error of the mean) compared to controls (49.14 cells/unit volume ±
156 4.53) (Figure 2A-B, 2D, $P<0.0005$, Mann-Whitney U Test). Importantly, we observed Dcp-1
157 positive cells in the proximal row of the lamina (Figure 2B; $N^{exp}=20/20$), which we never
158 observed in controls (Figure 2A, $N^{ctrl}=19/19$). Altogether these results showed that EGFR
159 activity in $xg^O$ induces the differentiation of L5 neurons, and proximal LPCs that fail to receive
160 appropriate cues from $xg^O$ die by apoptosis.
161
162 *$xg^O$ respond to EGF from photoreceptors and secrete multiple ligands to induce MAPK-*
163 *dependent neuronal differentiation of L5s.*
164 Since EGF from photoreceptors triggers EGFR activity in wrapping glia (Fernandes et
165 al., 2017), we tested whether photoreceptor-derived EGF contributed to activating EGFR in $xg^O$
166 also. Spi is initially produced as an inactive transmembrane precursor (mSpi) that needs to be
167 cleaved into its active secreted form (sSpi) (Tsruya et al., 2002). This requires the intracellular
168 trafficking protein Star and Rhomboid proteases (Tsruya et al., 2002; Urban et al., 2002; Yogev
169 et al., 2008). We took advantage of a mutant for *rhomboid 3 (rho3)* in which photoreceptors are
170 specified but cannot secrete EGF from their axons (Yogev et al., 2010), resulting in failure of
171 L1-L4 neurons to differentiate along with a significant decrease in the number of L5s (Figure
172 3A, 3C; $P^{rho3}<0.0001$; one-way ANOVA with Dunn's multiple comparisons test) (Fernandes et
173 al., 2017; Yogev et al., 2010). This result suggested that EGFR signalling in the $xg^O$ could be
174 activated by EGF secreted by photoreceptor axons. To test this hypothesis, we restored
175 expression of wild-type Rho3 only in photoreceptors in *rho3* mutant animals using a
176 photoreceptor-specific driver *(GMR-Gal4)*. Rho3 function in photoreceptors was sufficient to
177 fully rescue not only L1-L4 neuronal differentiation, as previously reported (Yogev et al., 2010),
178 but also L5 neuronal differentiation (Figure 3B, 3C; one-way ANOVA with Dunn's multiple
179 comparisons test). Since photoreceptor-derived EGF was insufficient to induce L5 neuronal
180 differentiation when EGFR signalling was blocked in $xg^O$ (Figure1 F,H), together these results
181 suggest that $xg^O$ likely respond to EGF from photoreceptors and relay these signals to induce
182 differentiation of proximal LPCs into L5 neurons.
183 We next asked what signal(s) the $xg^O$ secrete to induce L5 differentiation. Previously, we
184 showed that MAPK signalling is necessary and sufficient for neuronal differentiation in the

185 lamina (Fernandes et al., 2017). Therefore, we reasoned that $xg^O$-derived differentiation signal(s)
186 must activate MAPK signalling through a Receptor Tyrosine Kinase (RTK) in the proximal
187 lamina. Indeed, blocking EGFR signalling in $xg^O$ led to reduced levels of double phosphorylated
188 MAPK (dpMAPK) specifically in the proximal lamina (Figure 3 - Figure Supplement 1A, B).
189 The *Drosophila* genome encodes 22 ligands which activate 10 RTKs upstream of MAPK
190 signalling (Sopko and Perrimon, 2013). To identify the signal(s) secreted by $xg^O$, we
191 misexpressed candidate ligands and screened for their ability to rescue the loss of L5s caused by
192 blocking EGFR activity in the $xg^O$. To validate this approach, we tested whether autonomously
193 restoring transcriptional activity downstream of MAPK in $xg^O$ while blocking EGFR activity
194 could rescue L5 differentiation. While blocking EGFR in $xg^O$ resulted in laminas containing
195 0.063 ± 0.014 L5s per column, co-expressing PntP1 with $EGFR^{DN}$ in $xg^O$ rescued the number of
196 L5s per column to 0.213 ± 0.025 (Figure 3F, Figure 3 - Figure Supplement 1C P****<0.0001
197 compared to $EGFR^{DN}$ alone). We then screened 18 RTK ligands based on available reagents
198 (Figure 3 - Figure Supplement 1C). Four ligands, Spitz (Spi), Branchless (Bnl), Thisbe (Ths) and
199 Collagen type IV alpha 1 (Col4a1) produced statistically significant rescues when compared with
200 the $xg^O$>$EGFR^{DN}$+*CD8::GFP* (Gal4 titration control) (Figure 3- Figure Supplement 1C; P*<
201 0.05, P**<0.005, P***<0.0005, P****<0.0001 one-way ANOVA with Dunn's multiple
202 comparisons test). To eliminate false positive hits, we determined whether these ligands were
203 expressed in $xg^O$ under physiological conditions. Using a previously validated *bnl-Gal4* (Chen
204 and Krasnow, 2014; Kamimura et al., 2006; Spéder and Brand, 2014; Tamamouna et al., 2021),
205 we drove CD8::GFP expression and found that it was expressed in all cells of the optic lobe
206 (Figure 3 - Figure Supplement 1D), making it unlikely to be a viable hit. We found that a
207 previously validated *ths-Gal4* (Anllo and DiNardo, 2022; Wu et al., 2017) drove CD8::GFP
208 expression in photoreceptors but not $xg^O$ (Figure 3 - Figure Supplement 1E) consistent with
209 previous reports (Franzdóttir et al., 2009). However, when we examined *Col4a1* expression
210 using a previously validated Gal4 enhancer trap (Hennig et al., 2006), we found that it drove
211 CD8::GFP expression in $xg^O$ (Figure 3 - Figure Supplement 1F). We also found that a *spi-Gal4*
212 (NP0289-Gal4; not previously validated) drove CD8::GFP expression in $xg^O$, but not
213 photoreceptors or other cell types where *spi* is also known to be expressed, suggesting that this
214 Gal4 line may report *spi* expression partially (Figure 3 - Figure Supplement 1G). To further
215 substantiate these results we performed fluorescence *in situ* hybridisation chain reaction (HCR),

216 a form of fluorescent *in situ* hybridisation (Choi et al., 2018, 2016; Duckhorn et al., 2022), and
217 confirmed that *spi* and *Col4a1* mRNAs were present in the $xg^O$ under physiological conditions
218 (Figure 3 - Figure Supplement 1H, 1I; See Materials and Methods). This enabled us to narrow
219 down our hits to two ligands: the EGF Spi and Col4a1, a type IV collagen, which both rescued
220 L5 differentiation resulting in laminas with 0.147 ± 0.024 and 0.17 ± 0.0197 L5s per column,
221 respectively (Figure 3F-K, 3P $P^{spi\text{-}wt}$<0.01 and $P^{Col4a1}$ <0.0005, one-way ANOVA with Dunn's
222 multiple comparisons test; Figure 3- Figure Supplement 1C). Note that expressing either sSpi or
223 wild-type (unprocessed) mSpi (referred to as $Spi^{wt}$) in $xg^O$ rescued L5 numbers (Figure 3 –
224 Figure supplement 1C), indicating that $xg^O$ are capable of processing mSpi into the active form
225 (sSpi).
226 We ruled out the trivial explanation that the rescue of L5 numbers by Spi was caused by
227 autocrine EGFR reactivation in the $xg^O$, as Spi expression in $xg^O$ did not autonomously rescue
228 dpMAPK nuclear localisation when EGFR signalling was blocked (Figure 3 – Figure
229 Supplement 1A, B, J, K). We then tested whether $xg^O$ express *spi* and *Col4a1* downstream of
230 EGFR activity. We measured *spi* and *Col4a1* transcript levels using *in situ* HCR in controls and
231 when we blocked EGFR signalling in $xg^O$. Disrupting EGFR signalling in $xg^O$ resulted in a
232 significantly reduced fluorescence signal for *spi* and *Col4a1* transcripts in $xg^O$ compared with
233 controls (Figure 3- Figure Supplement 1H, 1I,1L-O; $P^{spi}$<0.01, $P^{Col4a1}$<0.005; Mann-Whitney U
234 Test). Thus, $xg^O$ express *spi* and *Col4a1* in response to EGFR activity.
235 Col4a1 is thought to activate MAPK signalling through its putative receptor, the
236 Discoidin domain receptor (Ddr) (Sopko and Perrimon, 2013). We used a Gal4 enhancer trap in
237 the *Ddr* locus (not previously validated) to drive CD8::GFP expression and observed that GFP
238 was expressed in all LPCs (Figure 3- Figure Supplement 1P). We confirmed these results using
239 *in situ* HCR, which also detected *Ddr* expression throughout the lamina (Figure 3 – Figure
240 supplement 1Q). Spi activates EGFR (Sopko and Perrimon, 2013), which was shown to be
241 expressed in LPCs previously (Huang et al., 1998). Thus, LPCs express the RTKs that make
242 them competent to respond to the EGF Spi and Col4a1 produced by $xg^O$. Moreover, expressing
243 *spi* or *Col4a1* in $xg^O$ in which EGFR signalling was blocked rescued dpMAPK signal in L5s,
244 indicating that, when expressed in $xg^O$, these ligands were sufficient to activate MAPK signalling
245 in the proximal lamina (Figure3-Figure Supplement R-T; P**<0.005, P****<0.0001; one-way
246 ANOVA with Dunn's multiple comparisons Test). Co-expressing Spi and Col4a1 in the

247 *xg$^{O}$>EGFR$^{DN}$* background led to an enhanced and statistically significant rescue relative to
248 individual ligand rescues alone, resulting in laminas with 0.267 ± 0.025 L5s per column (Figure
249 3L-P; P<0.0001, Mann-Whitney U Test). We also tested whether these ligands could induce
250 ectopic L5 differentiation when overexpressed in the xg$^{O}$. Overexpressing either Spi or Col4a1
251 resulted in a 19% ± 1.8 (P<0.05) and a 24% ± 4 (P<0.005) increase in the number of L5s per
252 column relative to controls, respectively (Figure 3Q-S). Thus, Spi and Col4a1 from xg$^{O}$ are
253 sufficient to induce L5 differentiation.
254 Next, to test whether xg$^{O}$-derived Spi and Col4a1 are normally required to induce L5
255 neuronal differentiation, we disrupted their expression specifically in xg$^{O}$. We used RNA
256 interference (RNAi) to knock down *spi* and *Col4a1* expression both individually and
257 simultaneously in xg$^{O}$ using previously validated lines (Chen et al., 2016; Csordás et al., 2020;
258 Louradour et al., 2017; Morante et al., 2013; Pastor-Pareja and Xu, 2011). While knocking down
259 *spi* led to a mild decrease in L5 numbers, which was not statistically significant, knocking down
260 *Col4a1* in the xg$^{O}$ led to a statistically significant decrease in L5s (0.78 ± 0.03 L5s per column)
261 relative to controls (0.92 ± 0.02 L5s per column) (Figure 3T, 3U, 3W; P*<0.05 one-way
262 ANOVA with Dunn's multiple comparisons test). However, knocking down both *spi* and *Col4a1*
263 simultaneously in xg$^{O}$ led to a strong decrease in L5s (0.61 ± 0.02 L5s per column; Figure 3V-
264 W; P****<0.0001,one-way ANOVA with Dunn's multiple comparisons test). Under these
265 conditions we also observed Dcp1 positive apoptotic cells in the most proximal row of the
266 lamina, which were never observed in controls (Figure 3- Figure supplement 2) but were
267 observed when L5 differentiation was blocked above (Figure 2B). Thus, xg$^{O}$-derived Spi and
268 Col4a1 are both necessary and sufficient to induce L5 differentiation. Altogether, we found that
269 xg$^{O}$ secrete multiple factors that lead to activation of the MAPK cascade in the proximal lamina
270 to induce differentiation of L5s.
271
272 *The 'extra' lamina precursor cells are specified as L5s though fated to die*
273 We recently showed that a gradient of Hh signalling activity in lamina columns specifies
274 L1-L5 identities such that high levels specify L2 and L3 (distal cell) identities, intermediate
275 levels specify L1 and L4 (intermediate cell) identities and low levels specify L5 (proximal cell)
276 identity (Bostock et al., 2022). Since overexpressing *spi* and *Col4a1* in the xg$^{O}$ resulted in
277 ectopic L5 neurons, we wondered what the source of these ectopic cells was. We quantified other

278 lamina neuron types when either *spi* or *Col4a1* was overexpressed in $xg^O$ and found no decrease
279 in the number of L1-L3s (Slp2-only expressing cells) or L4s (Bsh-only expressing cells) per
280 column compared to controls (Figure 3S). Thus, ectopic L5s were not produced at the expense of
281 other lamina neuron types. In wild-type optic lobes, each lamina column contains an 'extra'
282 LPC, which is located immediately distal to the LPC fated to differentiate as an L5. These 'extra'
283 LPCs do not differentiate but instead undergo apoptosis and are eliminated (Figure 2A and 4A).
284 We hypothesised that though fated to die, 'extra' LPCs are specified with L5 identity through
285 low Hh signalling activity in the proximal lamina, and that the overexpression of Spi and Col4a1
286 in $xg^O$ generated ectopic L5s by inducing differentiation and survival of the 'extra' LPCs. To test
287 this hypothesis, we forced neuronal differentiation throughout the lamina by expressing an
288 activated form of MAPK ($MAPK^{ACT}$) (Figure 4 – Figure Supplement 1A-D) or by
289 overexpressing the MAPK transcriptional effector, Pointed P1 (PntP1), in the lamina (Figure 4A-
290 D). As reported previously, hyperactivating MAPK signalling in the lamina led to premature
291 neuronal differentiation: instead of sequential differentiation of L1-L4, seen as a triangular front,
292 most lamina columns differentiated simultaneously (Figure 4C, Figure 4 - Figure supplement 1A,
293 C) (Fernandes et al., 2017). We observed no LPCs that remained undifferentiated ($Dac^+$ and
294 $Elav^-$) past lamina column 5, including the row of cells that normally correspond to the 'extra'
295 LPCs (Figure 4C, Figure 4 - Figure Supplement 1A, C). Importantly, we also observed a
296 concomitant decrease in cleaved Dcp-1 positive cells (Figure 4C, E ; $P<0.0001$, Mann-Whitney
297 U Test), suggesting that forcing the 'extra' LPCs to differentiate blocked their death.
298 Next, we examined the distribution of lamina neuron types when we forced neuronal
299 differentiation. We often observed two rows of cells co-expressing Slp2 and Bsh in the proximal
300 lamina (Figure 4B, D, Figure 4- figure supplement 1B, D), indicating the presence of ectopic
301 L5s. To distinguish between premature and ectopic differentiation, we quantified the number of
302 lamina neuron types (L1-L3, L4 and L5) per column in older columns (column 7 onwards, once
303 mature columns were observed in controls, Figure 4 - Figure Supplement 1E). While there was
304 no significant difference between the average number of L1-L3s or L4s per column, the average
305 number of L5s per column was ~1.4-fold higher in laminas in which differentiation was
306 ectopically induced compared with controls, *i.e.* they contained $1.4 \pm 0.08$ L5s per column
307 compared to $1.00 \pm 0.05$ L5s per column in controls (Figure 4B, D, F-G; $P<0.0001$, Mann-
308 Whitney U Test). Thus, hyperactivating MAPK signalling in the lamina drove ectopic

309 differentiation of L5 neurons. Importantly, ectopic L5s were only observed in the proximal but
310 never in the distal lamina (Figure 4D, N=18/18; Figure 4 - Figure Supplement 1D, N=9/9).
311 Taken together, the absence of cell death in the row distal to L5s and the presence of ectopic L5s
312 in this row indicate that hyperactivating MAPK signalling induces the 'extra' LPCs to
313 differentiate into L5s. Thus, the 'extra' LPCs are specified as L5s though fated to die normally.
314 These data are consistent with our work showing that lamina precursors are specified by Hh
315 signalling prior to differentiation and that the most proximal cells, which experience the lowest
316 levels of Hh pathway activity and are specified as L5s (Bostock et al., 2022). Importantly, the
317 presence of ectopic L5s when differentiation is induced demonstrates that more LPCs are
318 specified as L5s than differentiate normally.
319
320 *Newly born L5 neurons inhibit differentiation of distal neighbours to set neuronal number*
321 If the two most proximal cells in each lamina column are both specified as L5s, how then
322 is L5 differentiation limited to only the most proximal row in response to diffusible signals
323 secreted by $xg^{O}$? We tested whether the 'extra' LPCs differentiated as L5s when apoptosis was
324 blocked in animals mutant for *Death regulator Nedd2-like caspase (Dronc)*, an initiator caspase
325 essential for caspase-dependent cell death (Fuchs and Steller, 2011). Cleaved Dcp-1 was absent
326 in homozygous $Dronc^{I24}$ animals confirming that apoptosis was blocked (Figure 5A; N=26/26;
327 with full penetrance). Indeed, we detected cells that were positive for the lamina marker
328 Dachshund (Dac) but negative for the pan-neuronal marker Elav between L1-L4 and L5 neurons
329 past column 5, which were never observed in controls (Figure 5A compared to 4A; N=13/13;
330 with full penetrance). These cells did not express lamina neuron type markers Slp2 or Bsh, which
331 L5s co-express and which individually label L1-L3s and L4s, respectively (Figure 5B,C). Thus,
332 although the 'extra' LPCs were retained when apoptosis was blocked, they did not differentiate
333 into neurons.
334 We observed ectopic L5s only when all LPCs were forced to differentiate, bypassing the
335 need for differentiation signals from glia, but not when apoptosis was blocked (Figure 4C-D,
336 Figure 4-figure supplement 1A-D and Figure 5A-C). This suggests that the 'extra' LPCs, though
337 specified as L5s, did not receive differentiation signals from $xg^{O}$ in *Dronc* mutants or in the wild-
338 type, where failing to differentiate they were eliminated by apoptosis. How are only half of the
339 LPCs specified as L5s chosen to differentiate in an invariant manner? The most proximal row of

340 LPCs fated to differentiate into L5s is the row nearest to $xg^O$, and therefore, the first to receive
341 differentiation signals. We speculated that newly-induced L5s may then limit the ability of more
342 distal LPCs to differentiate, by preventing MAPK activation in neighbouring cells. Aos is a
343 transcriptional target of MAPK signalling and a secreted antagonist of the EGF Spi (Freeman et
344 al., 1992; Golembo et al., 1996). We wondered if newly-induced L5s secrete Aos to limit
345 differentiation signals from $xg^O$. To test this hypothesis, we examined *argos* (*aos*) expression
346 with an enhancer trap in the *aos* locus, $aos^{W11}$. *aos-lacZ* ($aos^{W11/+}$) was expressed in $xg^O$ and
347 differentiating lamina neurons, with the highest levels detected in L5s (Figure 5D-E).
348 Interestingly, we also noted ectopic L5s in the laminas of $aos^{W11}$ heterozygotes, which could be
349 the result of decreased Aos expression, as $aos^{W11}$ is a hypomorphic loss-of-function allele (Figure
350 5E). These observations suggested that Aos could act in L5s as a feedback-induced sink for Spi
351 to limit further differentiation in columns. To test this hypothesis, we knocked down *aos* by
352 RNAi using a driver expressed specifically in developing L5s (Jenett et al., 2012) (Figure 5G).
353 We observed a statistically significant ~1.2-fold increase in the number of L5s relative to
354 controls, *i.e.* 0.99 ± 0.02 L5s per column compared to 0.83 ± 0.01 L5s per column in controls
355 (Figure 5F-H; $P<0.0005$, Mann-Whitney U Test). Altogether, out data indicate a model in which
356 $xg^O$ induce MAPK activity in the most proximal LPCs, resulting in their differentiation and in
357 the production of the feedback inhibitor Aos. In turn, Aos limits further differentiation in the
358 column by fine-tuning the availability of the differentiation signal Spi, which ensures that only
359 one L5 differentiates per column, and determines the final number of neurons in each lamina
360 column.
361
362
363 **Discussion**
364 Appropriate circuit formation and function require that neuronal numbers are tightly
365 regulated. This is particularly important for the visual system, which is composed of repeated
366 modular circuits spanning multiple processing layers. In *Drosophila,* photoreceptors induce their
367 target field, the lamina, thus, establishing retinotopy between the compound eye and the lamina
368 (Huang and Kunes, 1996). Each lamina unit or column in the adult is composed of exactly 5
369 neurons; however, columns initially contain 6 LPCs. The sixth, or 'extra', LPC, invariantly
370 located immediately distal to the differentiating L5 neuron, is fated to die by apoptosis. These

371 ‘extra’ LPCs did not differentiate when apoptosis was blocked (Figure 5A,B) but generated
372 ectopic L5s when forced to differentiate (Figure 4D and Figure 4- figure supplement 1D).
373 Although we cannot rule out that preventing death using *Dronc* mutants may mis-specify the
374 ‘extra’ cells and prevent them from differentiating, it is more likely that these ‘extra’ cells are
375 specified as L5s, but that other mechanisms restricted their differentiation in *Dronc* mutants, as
376 other lamina neuron types differentiated normally (Figure 5B). Thus, twice as many LPCs appear
377 to be specified as L5s than undergo differentiation normally, which implies that a selection
378 process to ensure the correct number of L5s develop is in place.
379 The developmental strategies described thus far for setting neuronal number do so by
380 regulating proliferation of precursors and/or survival of differentiated neurons (Hidalgo, 2003).
381 Here, we have defined a unique strategy whereby L5 neuronal numbers are set by regulating how
382 many precursors from a larger pool are induced to differentiate, followed by programmed cell
383 death of the excess precursors. We showed that a glial population called $xg^O$, which are located
384 proximal to the lamina, secrete at least two ligands (Spi, Col4a1) that activate MAPK signalling
385 in LPCs to induce their differentiation (Figure 3, Figure 3 - Figure Supplement 1). The tissue
386 architecture is such that secreted signals from the $xg^O$ reach the most proximal row of LPCs first,
387 and therefore these precursors differentiate first. Upon differentiation, these newly induced
388 neurons secrete the Spi antagonist Aos to limit the available pool of Spi. As a result, the MAPK
389 pathway is not activated in the ‘extra’ L5 LPCs, preventing them from differentiating into L5
390 neurons (Figure 5). Intriguingly, L5 neuronal differentiation in the youngest columns of the
391 lamina proceeds despite Aos secretion by newly-induced L5s. We noted that differentiating L5s
392 expressed *aos* (based on *aos-lacZ*) at low levels initially and increased expression gradually till it
393 plateaued from column 5 onwards (Figure 5E and Figure 5 – Figure Supplement 1B). This delay
394 in high *aos* expression may thus enable differentiation of the youngest LPCs, while still
395 inhibiting differentiation of the row immediately distal. In sum, the structure of the tissue
396 together with feedback from newly induced neurons set neuronal number by limiting which and,
397 therefore, how many LPCs are induced to differentiate.
398
399 *Co-ordinating development through glia*
400 We have shown that in addition to the wrapping glia (Fernandes et al., 2017), another
401 population of glia, the $xg^O$, also receive and relay signals from photoreceptors to induce neuronal

402 differentiation in the lamina (Figure 1E-F). This is the first functional role ascribed to $xg^O$.
403 Remarkably, $xg^O$ are born from central brain DL1 type II neuroblasts and migrate into the optic
404 lobes to positions below the developing lamina (Ren et al., 2018; Viktorin et al., 2013). This
405 underscores an extraordinary degree of coordination and interdependence between the compound
406 eye, optic lobe and central brain. Photoreceptor signals drive wrapping glial morphogenesis and
407 infiltration into the lamina (Franzdóttir et al., 2009), thus setting the pace of L1-L4 neuronal
408 differentiation (Fernandes et al., 2017). Defining the signals that enable $xg^O$ to navigate the
409 central brain and optic lobe will be a critical contribution to our understanding of how
410 development is coordinated across brain regions.
411
412 *Tissue architecture sets up stereotyped programmed cell death*
413 In both vertebrate and invertebrate developing nervous systems, programmed cell death is
414 thought to come in two broad flavours: first as an intrinsically programmed fate whereby specific
415 lineages or identifiable progenitors, neurons or glia undergo stereotyped clearance (Hidalgo,
416 2003; Miguel-Aliaga and Thor, 2009; Pinto-Teixeira et al., 2016; Yamaguchi and Miura, 2015)
417 and second as an extrinsically controlled outcome of competition among neurons for limited
418 target-derived trophic factors, which adjust overall cell numbers through stochastic clearance
419 (also known as the neurotrophic theory) (Davies, 2003; Hidalgo, 2003; Miguel-Aliaga and Thor,
420 2009; Yamaguchi and Miura, 2015). In the lamina, although the LPCs eliminated by
421 programmed cell death are identifiable and the process stereotyped, it does not appear to be
422 linked to an intrinsic programme. Rather, the predictable and stereotyped nature of apoptosis and
423 differentiation are a consequence of stereotyped responses to extrinsic signalling determined by
424 the architecture of the tissue. Thus, our work highlights that stereotyped patterns of apoptosis can
425 arise from extrinsic signalling, suggesting a new mode to reliably pattern development of the
426 nervous system.
427 In many contexts, neurotrophic factors promote cell survival by activating MAPK
428 signalling (Ballif and Blenis, 2001; Park and Poo, 2013). In the lamina, MAPK-induced neuronal
429 differentiation and cell survival appear intimately linked. LPCs that do not activate MAPK
430 signalling sufficiently do not differentiate and are eliminated by apoptosis, likely through
431 regulation of the proapoptotic factor Head involution defective, which has been described
432 extensively in flies (Bergmann et al., 2002, 1998; Kurada and White, 1998). Thus, here the $xg^O$-

433 secreted ligands Spi and Col4a1, which activate MAPK, appear to be functioning as
434 differentiation signals as well as trophic factors. Col4a1, in particular, may perform dual roles by
435 promoting MAPK activity directly through its receptor Ddr, and perhaps also by limiting Spi
436 diffusivity to aid in localising MAPK activation.
437
438 It will be interesting to determine whether the processes described here represent
439 conserved strategies for regulating neuronal number. Certainly, given the diversity of cell types
440 and structural complexity of vertebrate nervous systems, exploiting tissue architecture would
441 appear to be an effective and elegant strategy to regulate cell numbers reliably and precisely.

442 **References**


443 Akagawa H, Hara Y, Togane Y, Iwabuchi K, Hiraoka T. 2015. The role of the effector caspases
444 drICE and dcp-1 for cell death and corpse clearance in the developing optic lobe in
445 Drosophila. *Dev Biol* 1–15. doi:10.1016/j.ydbio.2015.05.013

446 Amoyel M, Anderson J, Suisse A, Glasner J, Bach EA. 2016. Socs36E Controls Niche
447 Competition by Repressing MAPK Signaling in the Drosophila Testis. *PLoS Genet*
448 **12**:e1005815. doi:10.1371/journal.pgen.1005815

449 Anllo L, DiNardo S. 2022. Visceral mesoderm signaling regulates assembly position and
450 function of the Drosophila testis niche. *Dev Cell* **57**:1009-1023.e5.
451 doi:https://doi.org/10.1016/j.devcel.2022.03.009

452 Apitz H, Salecker I. 2014. A challenge of numbers and diversity: neurogenesis in the Drosophila
453 optic lobe. *J Neurogenet* **28**:1–35. doi:10.3109/01677063.2014.922558

454 Ballif BA, Blenis J. 2001. Molecular Mechanisms Mediating Mammalian Mitogen-activated
455 Protein Kinase (MAPK) Kinase (MEK)-MAPK Cell Survival Signals. *Cell Growth Differ*
456 **12**:397–408.

457 Bergmann A, Agapite J, McCall K, Steller H. 1998. The Drosophila gene hid is a direct
458 molecular target of Ras-dependent survival signaling. *Cell* **95**:331–41.

459 Bergmann A, Tugentman M, Shilo BZ, Steller H. 2002. Regulation of cell number by MAPK-
460 dependent control of apoptosis: A mechanism for trophic survival signaling. *Dev Cell*
461 **2**:159–170. doi:10.1016/S1534-5807(02)00116-8

462 Bostock MP, Prasad A, Donoghue A, Fernandes VM. 2022. Photoreceptors generate neuronal
463 diversity in their target field through a Hedgehog morphogen gradient in Drosophila. *Elife*
464 **11**:e78093. doi:10.1101/2022.02.21.481306

465 Chen F, Krasnow MA. 2014. Progenitor Outgrowth from the Niche in Drosophila Trachea Is
466 Guided by FGF from Decaying Branches. *Science (80- )* **343**:186–189.
467 doi:10.1126/science.1241442

468 Chen J, Xu N, Huang H, Cai T, Xi R. 2016. A feedback amplification loop between stem cells
469 and their progeny promotes tissue regeneration and tumorigenesis. *Elife* **5**:e14330.
470 doi:10.7554/eLife.14330

471 Choi HMT, Calvert CR, Husain N, Huss D, Barsi JC, Deverman BE, Hunter RC, Kato M, Lee
472 SM, Abelin ACT, Rosenthal AZ, Akbari OS, Li Y, Hay BA, Sternberg PW, Patterson PH,

473 Davidson EH, Mazmanian SK, Prober DA, Rijn M Van De, Leadbetter JR, Newman DK,
474 Readhead C, Bronner ME, Wold B, Lansford R, Sauka-spengler T, Fraser SE, Pierce NA.
475 2016. Mapping a multiplexed zoo of mRNA expression. *Development* **143**:3632–3637.
476 doi:10.1242/dev.140137
477 Choi HMT, Schwarzkopf M, Fornace ME, Acharya A, Artavanis G, Stegmaier J, Cunha A,
478 Pierce NA. 2018. Third-generation in situ hybridization chain reaction : multiplexed,
479 quantitative, sensitive, versatile, robust. *Development* **145**:dev165753.
480 doi:10.1242/dev.165753
481 Chotard C, Salecker I. 2007. Glial cell development and function in the Drosophila visual
482 system. *Neuron Glia Biol* **3**:17–25. doi:10.1017/S1740925X07000592
483 Csordás G, Grawe F, Uhlirova M. 2020. Eater cooperates with Multiplexin to drive the formation
484 of hematopoietic compartments. *Elife* **9**:e57297. doi:10.7554/eLife.57297
485 Davies AM. 2003. Regulation of neuronal survival and death by extracellular signals during
486 development. *EMBO J* **22**:2537–2545.
487 Duckhorn JC, Junker IP, Ding Y, Shirangi TR. 2022. Combined in Situ Hybridization Chain
488 Reaction and Immunostaining to Visualize Gene Expression in Whole-Mount Drosophila
489 Central Nervous Systems JuliaBehavioral Neurogenetics. Springer Nature.
490 doi:10.1007/978-1-0716-2321-3
491 Edwards TN, Nuschke AC, Nern A, Meinertzhagen I a. 2012. Organization and metamorphosis
492 of glia in the Drosophila visual system. *J Comp Neurol* **520**:2067–2085.
493 doi:10.1002/cne.23071
494 Fernandes VM, Chen Z, Rossi AM, Zipfel J, Desplan C. 2017. Glia relay differentiation cues to
495 coordinate neuronal development in Drosophila. *Science (80- )* **357**:886–891.
496 Fischbach KF, Dittrich APM. 1989. The optic lobe of Drosophila melanogaster. I: A. Golgi
497 analysis of wild-type structure. *Cell Tissue Res* **258**:441–475. doi:doi: 10.1007/BF00218858
498 Franzdóttir SR, Engelen D, Yuva-Aydemir Y, Schmidt I, Aho A, Klämbt C. 2009. Switch in
499 FGF signalling initiates glial differentiation in the Drosophila eye. *Nature* **460**:758–761.
500 doi:10.1038/nature08167
501 Freeman M, Klämbt C, Goodman CS, Rubin GM. 1992. The argos gene encodes a diffusible
502 factor that regulates cell fate decisions in the drosophila eye. *Cell* **69**:963–975.
503 doi:10.1016/0092-8674(92)90615-J

504 Fuchs Y, Steller H. 2011. Programmed Cell Death in Animal Development and Disease. *Cell*
505 **147**:742–758. doi:10.1016/j.cell.2011.10.033
506 Golembo M, Schweitzer R, Freeman M, Shilo B. 1996. argos transcription is induced by the
507 Drosophila EGF receptor pathway to form an inhibitory feedback loop. *Development*
508 **230**:223–230.
509 Hadjieconomou D, Timofeev K, Salecker I. 2011. A step-by-step guide to visual circuit
510 assembly in Drosophila. *Curr Opin Neurobiol* **21**:76–84. doi:10.1016/j.conb.2010.07.012
511 Hasegawa E, Kaido M, Takayama R, Sato M. 2013. Brain-specific-homeobox is required for the
512 specification of neuronal types in the Drosophila optic lobe. *Dev Biol* **377**:90–99.
513 doi:10.1016/j.ydbio.2013.02.012
514 Hennig KM, Colombani J, Neufeld TP. 2006. TOR coordinates bulk and targeted endocytosis in
515 the Drosophila melanogaster fat body to regulate cell growth . *J Cell Biol* **173**:963–974.
516 doi:10.1083/jcb.200511140
517 Hidalgo A. 2003. The control of cell number during central nervous system development in flies
518 and mice **120**:1311–1325. doi:10.1016/j.mod.2003.06.004
519 Huang Z, Kunes S. 1998. Signals transmitted along retinal axons in Drosophila: Hedgehog signal
520 reception and the cell circuitry of lamina cartridge assembly. *Development* **125**:3753–64.
521 doi:10.1016/s0092-8674(00)80094-x
522 Huang Z, Kunes S. 1996. Hedgehog, transmitted along retinal axons, triggers neurogenesis in the
523 developing visual centers of the Drosophila brain. *Cell* **86**:411–22. doi:10.1016/S0092-
524 8674(00)80114-2
525 Huang Z, Shilo BZ, Kunes S. 1998. A retinal axon fascicle uses spitz, an EGF receptor ligand, to
526 construct a synaptic cartridge in the brain of Drosophila. *Cell* **95**:693–703.
527 doi:10.1016/S0092-8674(00)81639-6
528 Jenett A, Rubin GM, Ngo T-TB, Shepherd D, Murphy C, Dionne H, Pfeiffer BD, Cavallaro A,
529 Hall D, Jeter J, Iyer N, Fetter D, Hausenfluck JH, Peng H, Trautman ET, Svirskas RR,
530 Myers EW, Iwinski ZR, Aso Y, DePasquale GM, Enos A, Hulamm P, Lam SCB, Li H-H,
531 Laverty TR, Long F, Qu L, Murphy SD, Rokicki K, Safford T, Shaw K, Simpson JH,
532 Sowell A, Tae S, Yu Y, Zugates CT. 2012. A GAL4-driver line resource for Drosophila
533 neurobiology. *Cell Rep* **2**:991–1001. doi:10.1016/j.celrep.2012.09.011
534 Kamimura K, Koyama T, Habuchi H, Ueda R, Masu M, Kimata K, Nakato H. 2006. Specific and

535 flexible roles of heparan sulfate modifications in Drosophila FGF signaling . *J Cell Biol*
536 **174**:773–778. doi:10.1083/jcb.200603129
537 Kurada P, White K. 1998. Ras Promotes Cell Survival in Drosophila by Downregulating hid
538 Expression **95**:319–329.
539 Louradour I, Sharma A, Morin-Poulard I, Letourneau M, Vincent A, Crozatier M, Vanzo N.
540 2017. Reactive oxygen species-dependent Toll/NF-κB activation in the Drosophila
541 hematopoietic niche confers resistance to wasp parasitism. *Elife* **6**:e25496.
542 doi:10.7554/eLife.25496
543 Luo L, Flanagan JG. 2007. Development of Continuous and Discrete Neural Maps. *Neuron*
544 **56**:284–300. doi:10.1016/j.neuron.2007.10.014
545 Malin J, Desplan C. 2021. Neural specification, targeting, and circuit formation during visual
546 system assembly. *Proc Natl Acad Sci* **118**:e21018231182. doi:10.1073/pnas.2101823118
547 Miguel-Aliaga I, Thor S. 2009. Programmed cell death in the nervous system — a programmed
548 cell fate ? *Curr Opin Neurobiol* **19**:127–133. doi:10.1016/j.conb.2009.04.002
549 Morante J, Vallejo DM, Desplan C, Dominguez M. 2013. Conserved miR-8/miR-200 Defines a
550 Glial Niche that Controls Neuroepithelial Expansion and Neuroblast Transition. *Dev Cell*
551 **27**:174–187. doi:10.1016/j.devcel.2013.09.018
552 Park H, Poo MM. 2013. Neurotrophin regulation of neural circuit development and function. *Nat*
553 *Rev Neurosci* **14**:7–23. doi:10.1038/nrn3379
554 Pastor-Pareja JC, Xu T. 2011. Shaping Cells and Organs in Drosophila by Opposing
555 Roles of Fat Body-Secreted Collagen IV and Perlecan. *Dev Cell* **21**:245–256.
556 doi:10.1016/j.devcel.2011.06.026
557 Pinto-Teixeira F, Konstantinides N, Desplan C. 2016. Programmed cell death acts at different
558 stages of Drosophila neurodevelopment to shape the central nervous system. *FEBS Lett*
559 **590**:2435–2453. doi:10.1002/1873-3468.12298.Programmed
560 Ren Q, Awasaki T, Wang Y, Huang Y, Lee T. 2018. Lineage-guided Notch-dependent
561 gliogenesis by Drosophila multi-potent progenitors. *Development* **145**:dev160127.
562 doi:10.1242/dev.160127
563 Schindelin J, Arganda-carreras I, Frise E, Kaynig V, Longair M, Pietzsch T, Preibisch S, Rueden
564 C, Saalfeld S, Schmid B, Tinevez J, White DJ, Hartenstein V, Eliceiri K, Tomancak P,
565 Cardona A. 2012. Fiji : an open-source platform for biological-image analysis. *Nat Methods*

566 **9**:676–682. doi:10.1038/nmeth.2019
567 Sopko R, Perrimon N. 2013. Receptor tyrosine kinases in Drosophila development. *Cold Spring*
568 *Harb Perspect Biol* **5**:a009050.
569 Spéder P, Brand AH. 2014. Gap junction proteins in the blood-brain barrier control nutrient-
570 dependent reactivation of Drosophila neural stem cells. *Dev Cell* **30**:309–321.
571 doi:10.1016/j.devcel.2014.05.021
572 Sugie A, Umetsu D, Yasugi T, Fischbach KF, Tabata T. 2010. Recognition of pre- and
573 postsynaptic neurons via nephrin/NEPH1 homologs is a basis for the formation of the
574 Drosophila retinotopic map. *Development* **137**:3303–3313. doi:10.1242/dev.047332
575 Tamamouna V, Rahman MM, Petersson M, Charalambous I, Kux K, Mainor H, Bolender V,
576 Isbilir B, Edgar BA, Pitsouli C. 2021. Remodelling of oxygen-transporting tracheoles drives
577 intestinal regeneration and tumorigenesis in Drosophila. *Nat Cell Biol* **23**:497–510.
578 doi:10.1038/s41556-021-00674-1
579 Tan L, Zhang KX, Pecot MY, Nagarkar-Jaiswal S, Lee PT, Takemura SY, McEwen JM, Nern A,
580 Xu S, Tadros W, Chen Z, Zinn K, Bellen HJ, Morey M, Zipursky SL. 2015. Ig Superfamily
581 Ligand and Receptor Pairs Expressed in Synaptic Partners in Drosophila. *Cell* **163**:1756–
582 1769. doi:10.1016/j.cell.2015.11.021
583 Treisman JE. 2013. Retinal differentiation in Drosophila. *Wiley Interdiscip Rev Dev Biol* **2**:545–
584 557. doi:10.1002/wdev.100
585 Tsruya R, Schlesinger A, Reich A, Gabay L, Sapir A, Shilo B. 2002. Intracellular trafficking by
586 Star regulates cleavage of the Drosophila EGF receptor ligand Spitz. *Genes Dev* **12**:222–
587 234. doi:10.1101/gad.214202.fate
588 Umetsu D, Murakami S, Sato M, Tabata T. 2006. The highly ordered assembly of retinal axons
589 and their synaptic partners is regulated by Hedgehog/Single-minded in the Drosophila
590 visual system. *Development* **133**:791–800. doi:10.1242/dev.02253
591 Urban S, Lee JR, Freeman M. 2002. A family of rhomboid intramembrane proteases activates all
592 Drosophila membrane-tethered EGF ligands. *EMBO J* **21**:4277–4286.
593 doi:10.1093/emboj/cdf434
594 Viktorin G, Riebli N, Reichert H. 2013. A multipotent transit-amplifying neuroblast lineage in
595 the central brain gives rise to optic lobe glial cells in Drosophila. *Dev Biol* **379**:182–194.
596 doi:10.1016/j.ydbio.2013.04.020

597 Wu B, Li J, Chou Y, Luginbuhl D, Luo L. 2017. Fibroblast growth factor signaling instructs
598 ensheathing glia wrapping of Drosophila olfactory glomeruli. *Proc Natl Acad Sci*
599 **114**:7505–7512. doi:10.1073/pnas.1706533114
600 Yamaguchi Y, Miura M. 2015. Review Programmed Cell Death in Neurodevelopment. *Dev Cell*
601 **32**:478–490. doi:10.1016/j.devcel.2015.01.019
602 Yogev S, Schejter ED, Shilo B-Z. 2008. Drosophila EGFR signalling is modulated by
603 differential compartmentalization of Rhomboid intramembrane proteases. *EMBO J*
604 **27**:1219–1230. doi:https://doi.org/10.1038/emboj.2008.58
605 Yogev S, Schejter ED, Shilo BZ. 2010. Polarized secretion of drosophila EGFR ligand from
606 photoreceptor neurons is controlled by ER localization of the ligand-processing machinery.
607 *PLoS Biol* **8**:e1000505.
608 Zang Y, Wan M, Liu M, Ke H, Ma S, Liu L, Pastor-pareja C. 2015. Plasma membrane
609 overgrowth causes fibrotic collagen accumulation and immune activation in Drosophila
610 adipocytes. *Elife* **4**:e07187. doi:10.7554/eLife.07187
611

612 **Acknowledgements:**
613 We thank C. Desplan, A. Gould, B. Shilo and J. Treisman for reagents, and S. Ackerman, M.
614 Amoyel, B. Conradt, C. Desplan, C. Doe, A. Franz, P. Salinas, A. Rossi, C. Stern, L.
615 Venkatasubramanian and members of the Amoyel and Fernandes labs for comments on the
616 manuscript. Stocks obtained from the Bloomington Drosophila Stock Center (NIH
617 P40OD018537) were used in this study. Monoclonal antibodies obtained from the
618 Developmental Studies Hybridoma Bank, created by the NICHD of the NIH and maintained at
619 The University of Iowa, were used in this study.
620
621 **Funding:**
622 Wellcome Trust Sir Henry Dale Research Fellowship 210472/Z/18/Z (VMF), UCL Overseas
623 Research Scholarship (ARP) and UCL Graduate Research Scholarship (ARP).
624
625 **Competing interests:**
626 The authors declare no competing interests.
627

**Author contributions:**

Conceptualization: VMF, ARP

Investigation: ARP, MPB, ILB, ZH, VMF

Supervision: VMF

Writing – original draft: VMF, ARP

Writing – review & editing: ARP, ILB

635 **Materials and Methods**

| **Key Resources Table** | | | | |
|---|---|---|---|---|
| **Reagent type (species) or resource** | **Designation** | **Source or reference** | **Identifiers** | **Additional information** |
| Genetic reagent (*D. melanogaster*) | *Canton S* | Bloomington Drosophila Stock Center | BDSC: 64349 | |
| Genetic reagent (*D. melanogaster*) | *Bacc-GFP* | Bloomington Drosophila Stock Center | BDSC: 36349 | |
| Genetic reagent (*D. melanogaster*) | *ey-Gal80* | Bloomington Drosophila Stock Center | BDSC: 35822 | |
| Genetic reagent (*D. melanogaster*) | *Gal80$^{ts}$* | Bloomington Drosophila Stock Center | BDSC: 7108 | |
| Genetic reagent (*D. melanogaster*) | *Dronc$^{I24}$* | PMID: 15800001 | | Gift from M. Amoyel |
| Genetic reagent (*D. melanogaster*) | *R27G05-Gal4* | Bloomington Drosophila Stock Center | BDSC: 48073 | Lamina Gal4 |
| Genetic reagent (*D. melanogaster*) | *R25A01-Gal4* | Bloomington Drosophila Stock Center | BDSC: 49102 | xg$^{O}$ Gal4 |
| Genetic reagent (*D. melanogaster*) | *R64B07-Gal4* | Bloomington Drosophila Stock Center | BDSC: 71106 | Larval L5 Gal4 |
| Genetic reagent (*D. melanogaster*) | *hh-gal4* | Bloomington Drosophila Stock Center | BDSC: 67493 | |
| Genetic reagent (*D. melanogaster*) | *Repo-Gal4* | Bloomington Drosophila Stock Center | BDSC: 7415 | |
| Genetic reagent (*D. melanogaster*) | *UAS-CD8::GFP* | Bloomington Drosophila Stock Center | BDSC: 32187 | |
| Genetic reagent (*D. melanogaster*) | *UAS-nls.lacZ* | Bloomington Drosophila Stock Center | BDSC: 3956 | |

| | | | | |
|---|---|---|---|---|
| Genetic reagent (*D. melanogaster*) | *GMR-Gal4* | Bloomington Drosophila Stock Center | BDSC: 9146 | |
| Genetic reagent (*D. melanogaster*) | *Repo-QF* | Bloomington Drosophila Stock Center | BDSC: 66477 | |
| Genetic reagent (*D. melanogaster*) | *NP6293-Gal4* | Kyoto Stock Center | DGRC: 105188 | Perineural Glia |
| Genetic reagent (*D. melanogaster*) | *NP2276-Gal4* | Kyoto Stock Center | DGRC: 112853 | Subperineur-al Glia |
| Genetic reagent (*D. melanogaster*) | *R54H02-Gal4* | Bloomington Drosophila Stock Center | BDSC: 45784 | Cortex Glia |
| Genetic reagent (*D. melanogaster*) | *R10C12-Gal4* | Bloomington Drosophila Stock Center | BDSC: 47841 | Epithelial and marginal glia |
| Genetic reagent (*D. melanogaster*) | *Mz97-Gal4* | Bloomington Drosophila Stock Center | BDSC: 9488 | Wrapping glia and $xg^{O}$ |
| Genetic reagent (*D. melanogaster*) | *R53H12-Gal4* | Bloomington Drosophila Stock Center | BDSC: 50456 | Chiasm glia |
| Genetic reagent (*D. melanogaster*) | $spi^{NP0289}$-*Gal4* | Kyoto Stock Center | DGRC: 112828 | |
| Genetic reagent (*D. melanogaster*) | *Cg-Gal4* | Bloomington Drosophila Stock Center | BDSC: 7011 | |
| Genetic reagent (*D. melanogaster*) | $bnl^{NP2211}$-*Gal4* | Kyoto Stock Center | DGRC: 112825 | |
| Genetic reagent (*D. melanogaster*) | $ths^{MI07139}$-*Gal4* | Bloomington Drosophila Stock Center | BDSC: 77475 | |
| Genetic reagent (*D. melanogaster*) | $rho3^{PLLb}$, *UAS-CD8::GFP* | PMID: 20957186 | | Gift from B. Shilo |
| Genetic reagent (*D. melanogaster*) | *UAS-rho3-3xHA* | PMID: 20957186 | | Gift from B. Shilo |
| Genetic reagent (*D. melanogaster*) | $aos^{w11}$ | Bloomington Drosophila Stock Center | BDSC: 2513 | *aos-lacZ* |

| | | | | |
|---|---|---|---|---|
| Genetic reagent (*D. melanogaster*) | *BaccGFP;10x QUAS-6xmCherry-HA* | Bloomington Drosophila Stock Center | BDSC: 55270 | |
| Genetic reagent (*D. melanogaster*) | *10xUAS-myrGFP* | Bloomington Drosophila Stock Center | BDSC: 32197 | |
| Genetic reagent (*D. melanogaster*) | *UAS-LifeAct-GFP* | Bloomington Drosophila Stock Center | BDSC: 35544 | |
| Genetic reagent (*D. melanogaster*) | *UAS-Dicer2* | Bloomington Drosophila Stock Center | BDSC: 24650 | |
| Genetic reagent (*D. melanogaster*) | *;UAS-EGFR$^{DN}$; UAS-EGFR$^{DN}$* | Bloomington Drosophila Stock Center | BDSC: 5364 | |
| Genetic reagent (*D. melanogaster*) | *UAS-rl$^{SEM}$* | Bloomington Drosophila Stock Center | BDSC: 59006 | *rl$^{SEM}$=MAPK$^{ACT}$* |
| Genetic reagent (*D. melanogaster*) | *UAS-PntP1* | Bloomington Drosophila Stock Center | BDSC: 869 | |
| Genetic reagent (*D. melanogaster*) | *UAS-jeb* | PMID: 21816278 | | Gift from A. Gould |
| Genetic reagent (*D. melanogaster*) | *UAS-Col4a1$^{EY11094}$* | Bloomington Drosophila Stock Center | BDSC: 20661 | |
| Genetic reagent (*D. melanogaster*) | *UAS-Cg25cRFP* | PMID: 26090908 | | Gift from A. Franz *Cg25c = Col4a1* |
| Genetic reagent (*D. melanogaster*) | *UAS-wnt5* | Bloomington Drosophila Stock Center | BDSC: 64298 | |
| Genetic reagent (*D. melanogaster*) | *UAS-s.spi* | PMID: 7601354 | | Gift from B. Shilo |
| Genetic reagent (*D. melanogaster*) | *UAS-m.spi::GFP-myc (II)* | PMID: 11799065 | | Gift from B. Shilo *m.spi = spi$^{wt}$* |
| Genetic reagent (*D. melanogaster*) | *UAS-m.spi::GFP-myc (III)* | PMID: 11799065 | | Gift from B. Shilo *m.spi = spi$^{wt}$* |

| | | | | |
|---|---|---|---|---|
| Genetic reagent (*D. melanogaster*) | *UAS-grk.sec* | Bloomington Drosophila Stock Center | BDSC: 58417 | |
| Genetic reagent (*D. melanogaster*) | *UAS-vn$^{EPgy}$* | Bloomington Drosophila Stock Center | BDSC: 58498 | |
| Genetic reagent (*D. melanogaster*) | *UAS-krn-3xHA* | FlyORF | F002754 | |
| Genetic reagent (*D. melanogaster*) | *UAS-bnl* | Bloomington Drosophila Stock Center | BDSC: 64232 | |
| Genetic reagent (*D. melanogaster*) | *UAS-Ilp1* | PMID: 12176357 | | Gift from P. Leopold |
| Genetic reagent (*D. melanogaster*) | *UAS-Ilp6* | PMID: 20059956 | | Gift from P. Leopold |
| Genetic reagent (*D. melanogaster*) | *UAS-Pvf1$^{XP}$* | Bloomington Drosophila Stock Center | BDSC: 19632 | |
| Genetic reagent (*D. melanogaster*) | *UAS-Pvf2$^{XP}$* | Bloomington Drosophila Stock Center | BDSC: 19631 | |
| Genetic reagent (*D. melanogaster*) | *UAS-Wnt4$^{EPgy2}$* | Bloomington Drosophila Stock Center | BDSC: 20162 | |
| Genetic reagent (*D. melanogaster*) | *UAS-boss-3xHA* | FlyORF | F001365 | |
| Genetic reagent (*D. melanogaster*) | *SAM.dCas9.Trk* | Bloomington Drosophila Stock Center | BDSC: 81322 | |
| Genetic reagent (*D. melanogaster*) | *SAM.dCas9.Pvf3* | Bloomington Drosophila Stock Center | BDSC: 81346 | |
| Genetic reagent (*D. melanogaster*) | *SAM.dCas9.ths* | Bloomington Drosophila Stock Center | BDSC: 81347 | |
| Genetic reagent (*D. melanogaster*) | *SAM.dCas9.pyr* | Bloomington Drosophila Stock Center | BDSC: 81330 | |
| Genetic reagent (*D. melanogaster*) | *Ddr$^{CR01018}$-Gal4* | Bloomington Drosophila Stock Center | BDSC: 81157 | |

| | | | | |
|---|---|---|---|---|
| Genetic reagent (*D. melanogaster*) | *spi*$^{RNAi}$ | Vienna Drosophila Stock Center | GD3922 | |
| Genetic reagent (*D. melanogaster*) | *Col4a1*$^{RNAi}$ | Vienna Drosophila Stock Center | GD28369 | |
| Genetic reagent (*D. melanogaster*) | *aos*$^{RNAi}$ | Vienna Drosophila Stock Center | GD47181 | |
| Antibody | anti-Dac2-3 (mouse monoclonal) | Developmental Studies Hybridoma Bank | mAbdac2-3 | 1:20 |
| antibody | anti-Repo (mouse monoclonal) | Developmental Studies Hybridoma Bank | 8D12 | 1:20 |
| antibody | anti-Elav (rat monoclonal) | Developmental Studies Hybridoma Bank | 7E8A10 | 1:100 |
| antibody | anti-Elav (mouse monoclonal) | Developmental Studies Hybridoma Bank | 9F8A9 | 1:20 |
| antibody | anti-Svp (mouse monoclonal) | Developmental Studies Hybridoma Bank | 6F7 | 1:50 |
| antibody | anti-Slp2 (guinea pig monoclonal) | PMID: 23783517 | C. Desplan | 1:100 |
| antibody | anti-Bsh (Rabbit monoclonal) | PMID: 33149298 | C. Deslpan | 1:500 |
| antibody | anti-dcp1 (Rabbit monoclonal) | Cell signalling | 9578 | 1:100 |
| antibody | anti-Brp (guinea-pig monoclonal) | | C. Desplan | 1:100 |

| | | | | |
|---|---|---|---|---|
| antibody | Anti-phospho-p44/42-MAPK (Thr202/Tyr 204) (Rabbit monoclonal) | Cell signalling | 9101 | 1:100 |
| antibody | anti b-galactosidase (mouse monoclonal) | Promega | #Z3781 | 1:500 |
| antibody | anti b-galactosidase (chicken monoclonal) | abcam | 9361 | 1:500 |
| antibody | anti-GFP (chicken monoclonal) | EMD Millipore | GFP-1010 | 1:400 |
| antibody | anti-pdm3 (rat monoclonal) | PMID: 22190420 | C. Desplan | 1:20 |
| antibody | anti-RFP (chicken monoclonal) | Rockland | #600-901-379s | 1:500 |
| antibody | anti-GFP (rabbit monoclonal) | Thermofisher | #A6455 | 1:500 |
| antibody | AlexaFluor405-conjugated Goat Anti-HRP | Jackson Immunolabs | 123-475-021 | 1:200 |
| antibody | AlexaFluorCy3-conjugated Goat Anti-HRP | Jackson Immunolabs | 11 23-165-021 | 1:200 |
| antibody | AlexaFluor647-conjugated Goat Anti-HRP | Jackson Immunolabs | 123-605-021 | 1:200 |

| | | | | |
|---|---|---|---|---|
| Sequence-based reagent | Antisense probe pairs for *in situ* Hybridization chain reaction | This study. *"Prasad et al HCR Probe Sequences.xls"* | DNA Oligos | Supporting Zip Document 1 |
| Software, algorithm | RStudio | RStudio | R version 4.0.3 | |
| software, algorithm | GraphPad Prism 9 | GraphPad Prism 9 | GraphPad Prism version 9.4.1 | |
| software, algorithm | Adobe Photoshop | Adobe Photoshop | Adobe Photoshop 2021 | |
| software, algorithm | Adobe Illustrator | Adobe Illustrator | Adobe Illustrator 2021 | |
| software, algorithm | Imaris | Imaris | Imaris x64-9.5.1 | |
| software, algorithm | FiJi, ImageJ | PMID: 22743772 | | |
| Chemical compound, drug | HCR Amplification Buffer | Molecular Instruments | BAM02224 | |
| Chemical compound, drug | HCR Wash Buffer | Molecular Instruments | BPW02124 | |
| Chemical compound, drug | HCR Hybridization Buffer | Molecular Instruments | BPH02224 | |
| Chemical compound, drug | HCR Amplifier B3-H1-546 | Molecular Instruments | S030724 | |

| | | | | |
|---|---|---|---|---|
| Chemical compound, drug | HCR Amplifier B3-H2-546 | Molecular Instruments | S031024 | |
| Chemical compound, drug | HCR Amplifier B3-H1-647 | Molecular Instruments | S040124 | |
| Chemical compound, drug | HCR Amplifier B3-H2-647 | Molecular Instruments | S040224 | |
| Chemical compound, drug | Para-formaldehyde | Fisher Scientific | 28908 | 4% solution |
| Chemical compound, drug | DAPI stain | Sigma | D9542-1MG | (1 µg/mL) |

636

637 <u>*Drosophila stocks and maintenance:*</u>

638 *Drosophila melanogaster* strains and crosses were reared on standard cornmeal medium and
639 raised at 25$^{O}$C or 29$^{O}$C or shifted from 18$^{O}$C to 29$^{O}$C for genotypes with temperature sensitive
640 Gal80, as indicated in Supporting File 2.

641 We used the following mutant and transgenic flies in combination or recombined in this study
642 (See Supporting File 2 for more details; {} enclose individual genotypes, separated by commas):
643 *{y,w,hsflp$^{122}$; sp/Cyo; TM2/TM6B}, {y,w; sp/Cyo, Bacc-GFP; Dr/TM6C},* (from BDSC: 36349)
644 *{ey-Gal80; sp/Cyo;}* (BDSC: 35822), *{;Gal80$^{ts}$; TM2/TM6B}* (BDSC: 7108), *{w$^{1118}$;; R27G05-*
645 *Gal4}* (BDSC: 48073), *{w$^{1118}$;;25A01-Gal4}* (BDSC: 49102), *{y,w; R64B07-Gal4;}* (larval L5-
646 Gal4), {y,w; hh-Gal4/TM3} (BDSC: 67493), *{;tub-Gal80$^{ts}$; repo-Gal4/TM6B}, {w$^{1118}$;GMR-*
647 *Gal4/Cyo;}* (BDSC: 9146), *{y,w;Pin/Cyo;repo-QF/TM6B}* (BDSC: 66477), *{y,w; NP6293-*
648 *Gal4/Cyo,UAS-lacZ;}* (perineurial glia; Kyoto Stock Center: 105188), *{w; NP2276-Gal4/Cyo; }*
649 (subperineurial glia; Kyoto Stock Center: 112853), *{w$^{1118}$;; R54H02-Gal4}* (cortex glia; BDSC:
650 45784), *{w$^{1118}$;; R10C12-Gal4}* (epithelial and marginal glia; BDSC: 47841), *{w;Mz97-Gal4,*
651 *UAS-Stinger/Cyo;}* (wrapping and xg$^{O}$; BDSC: 9488), *{w$^{1118}$;; R53H12-Gal4}* (chiasm glia;
652 BDSC: 50456), *{y,w; spi$^{NP0289}$-Gal4/Cyo, UAS-lacZ;}* (Kyoto Stock Center: 112128), *{w$^{1118}$; Cg-*
653 *Gal4;}* (BDSC: 7011), *{w;; bnl$^{NP2211}$-Gal4}* (Kyoto Stock Center: 112825), *{w; ths$^{MI07139}$-*
654 *Gal4/Cyo; MKRS/TM6B}* (BDSC: 77475), *{;;rho3$^{PLLb}$, UAS-CD8::GFP/TM6B}, {;UAS-rho3-*

655 *3xHA;}* (gifts from B. Shilo), *{;;aos$^{w11}$/TM6B}* (*aos-lacZ*; BDSC: 2513), *{y,w; sp/Cyo, Bacc-*
656 *GFP; 10xQUAS-6xmCherry-HA}* (BDSC: 52270), *{y,w;;10xUAS-myrGFP}* (BDSC: 32197),
657 *{;UAS-CD8::GFP;}, {;;UAS-CD8::GFP}* (gifts from C. Desplan)*, {y,w;;UAS-nls.lacZ},* (BDSC:
658 3956)*, {y,w; UAS-LifeAct-GFP/Cyo;}* (BDSC: 35544)*, {w$^{1118}$;UAS-Dcr-2;}* (BDSC: 24650),
659 *{w$^{1118}$;;UAS-Dcr-2}* (BDSC: 24651), *{;UAS-EGFR$^{DN}$; UAS-EGFR$^{DN}$}* (BDSC: 5364)*, {;UAS-*
660 *aop$^{ACT}$;}* (Kyoto Stock Center: 108425), *{y,w;UAS-rl$^{sem}$;}* (rl$^{sem}$ = MAPK$^{ACT}$; BDSC: 59006),
661 *{w$^{1118}$;;UAS-PntP1}* (BDSC: 869), *{w$^{1118}$;UAS-aos$^{RNAi}$;}* (VDRC47181), *{w;UAS-jeb;}* (a gift
662 from A. Gould), *{y,w, UAS-Col4a1$^{EY11094}$/(Cyo);}* (BDSC: 20661), *{;;UAS-Cg25c-RFP}* (Zang et
663 al., 2015) *(Col4a1 = Cg25c)*, *{;UAS-Wnt5;}* (BDSC: 64298), *{;;UAS-s.spi}* (a gift from B.
664 Shilo), *{;UAS-m.spi::GFP-myc;}* (a gift from B. Shilo), *{;;UAS-m.spi::GFP-myc}* (a gift from B.
665 Shilo), *{w, UAS-grk.sec/Cyo;}* (BDSC: 58417), *{;UAS-vn$^{EPgy}$/Cyo;}* (BDSC: 58498), *{;;UAS-*
666 *krn-3xHA}* (FlyORF: F002754), *{;UAS-bnl/Cyo; MKRS/TM6C}* (BDSC: 64232), *{;UAS-Ilp1;},*
667 *{;UAS-Ilp6;}* (gifts from P. Leopold), *{w$^{1118}$, UAS-Pvf1$^{XP}$;;}* (BDSC: 19632), *{w$^{1118}$; UAS-*
668 *Pvf2$^{XP}$;}* (BDSC: 19631), *{;UAS-Wnt4$^{EPgy2}$/Cyo;}* (BDSC: 20162), *{;;UAS-boss-3xHA}*
669 (FlyORF: F001365), *{y,sev; SAM.dCas9.Trk;}* (BDSC: 81322), *{y,sev; SAM.dCas9.Pvf3;}*
670 (BDSC: 81346), *{y,sev; SAM.dCas9.ths;}* (BDSC: 81347), *{y,sev; SAM.dCas9.pyr;}* (BDSC:
671 81330), *{w$^{1118}$; Ddr$^{CR01018}$-Gal4;}* (BDSC: 81157).
672
673 <u>*Immunocytochemistry, antibodies and microscopy:*</u>
674 We dissected eye-optic lobe complexes from early pupae (0-5hrs after puparium formation;
675 APF) in 1X phosphate-buffered saline (PBS), fixed in 4% formaldehyde for 20 minutes, blocked
676 in 5% normal donkey serum and incubated in primary antibodies diluted in block for 2 nights at
677 4$^{o}$C. Samples were then washed in 1X PBS with 0.5% TritonX (PBSTx), incubated in secondary
678 antibodies diluted in block, washed in PBSTx and mounted in SlowFade (Life Technologies).
679 When performing phospho-MAPK stains, dissections were performed in a phosphatase inhibitor
680 buffer as detailed in (Amoyel et al., 2016).
681
682 We used the following primary antibodies in this study: mouse anti-Dac$^{2-3}$ (1:20, Developmental
683 Studies Hybridoma Bank; DSHB), mouse anti-Repo (1:20, DSHB), rat anti-Elav (1:100, DSHB),
684 mouse anti-Elav (1:20, DSHB), rabbit anti-Dcp-1 (1:100; Cell Signalling #9578), chicken anti-
685 GFP (1:400; EMD Millipore), mouse anti-Svp (1:50, DSHB), rabbit anti-Slp2 (1:100; a gift from

686 C. Desplan), rabbit-Bsh (1:500; a gift from C. Desplan), Rat anti-Pdm3 (1:1000; a gift from C.
687 Desplan), guinea pig anti-Brp (1:100; a gift from C. Desplan), rabbit anti-Phospho-p44/42
688 MAPK (Erk1/2) (Thr202/Tyr204) (1:100, Cell Signaling #9101), chicken anti-RFP (1:500;
689 Rockland #600-901-379s), mouse anti β-galactosidase (1:500; Promega # Z3781), chicken anti
690 β-galactosidase (1:500; abcam #9361), rabbit-anti-GFP (1:500; Thermofisher #A6455),
691 AlexaFluor405 conjugated Goat Anti-HRP (1:100; Jackson Immunolabs), AlexaFluor405-, Cy3-,
692 or AlexaFluor647- conjugated Goat Anti-HRP (1:200; Jackson Immunolabs). Secondary
693 antibodies were obtained from Jackson Immunolabs or Invitrogen and used at 1:800. Images
694 were acquired using Zeiss 800 and 880 confocal microscopes with 40X objectives.
695
696 *In-situ Hybridisation Chain reaction:*
697 To determine if *spi, Col4a1 and Ddr* transcripts were present in the $xg^{O}$, we performed HCR as
698 detailed in Duckhorn et al. (2022). We designed 20-21 probe pairs against target genes,
699 excluding regions of strong similarity to other transcripts, with corresponding initiator sequences
700 for amplifiers B3 (Choi et al., 2018). HCR probes (sequences included as source data See
701 Supporting Zip Document 1) were purchased as DNA Oligos from ThermoFisher (100µm in
702 water and frozen).
703 Eye-optic lobe complexes were dissected, fixed and washed as detailed above. Samples were
704 incubated in Probe Hybridisation Buffer for 30 minutes at 37°C followed by incubation with
705 probes (0.01µM) at 37°C overnight. The samples were then washed four times for 15 minutes
706 each with probe wash buffer at 37°C followed by two washes for 5 minutes each with 5X saline
707 sodium citrate solution (20XSSCT solution in distilled water-- 58.44g/mol sodium chloride,
708 294.10g/mol 560 sodium citrate, pH adjusted to 7 with 14N hydrochloric acid, with 0.001%
709 Tween 20) at room temperature. Samples were then incubated with amplification buffer for 10
710 minutes at room temperature. 12 pmol of hairpins H1 and H2 were snap-cooled (95°C for 90
711 seconds and then cooled to room-temperature for 20 mins) separately to avoid oligomerisation.
712 The snap-cooled hairpins were then added to the samples in the amplification buffer (protected
713 from light) and incubated overnight at room temperature. The samples were then washed with
714 5XSSCT for 15 minutes before being incubated in darkness with 1:15 dilution of DAPI (Sigma
715 D9542) for 90 minutes. Samples were washed with 1xPBS for 30 minutes and then mounted as
716 detailed above.

717 *Quantification and Statistical analyses:*
718 We used Fiji-ImageJ (Schindelin et al., 2012) or Imaris (version x64-9.5.1) to process and
719 quantify confocal images as described below. We used Adobe Photoshop and Adobe Illustrator
720 software to prepare figures. We used GraphPad Prism8 to perform statistical tests. In all graphs,
721 whiskers indicate the standard error of the mean (SEM).
722 *Dcp-1 quantifications:*
723 We used the surfaces tool in Imaris to manually select the lamina region (based on Dac
724 expression). We then used the spots tool to identify Dcp-1 positive cells (cell diameter = 5μm)
725 within the selected region using the default thresholding settings, and plotted these values
726 normalised to the volume of the selected lamina region in GraphPad Prism8.
727
728 *Cell-type quantifications:*
729 *LPCs per column:* Column number was identified by counting HRP-labelled photoreceptor axon
730 bundles. We considered the youngest column located adjacent to the lamina furrow to be the first
731 column, with column number (age) increasing towards the posterior (right) of the furrow. We
732 counted the number of Dac+ cells per column by quantifying 10 optical slices (step size = 1μm)
733 located centrally in the lamina.
734
735 *Control* vs. *Lamina$^{ts}$>PntP1:* We quantified the lamina neuron types per column using the
736 following markers to identify L-neuron types: Elav+ and Slp2+ cells were counted as L1-L3s;
737 Elav+ and Bsh+ cells were counted as L4s and Elav+, Bsh+ and Slp2+ cells were counted as
738 L5s. We quantified 10 optical slices (step size = 1μm) located centrally in the lamina. Column
739 number was identified by counting HRP-labelled photoreceptor axon bundles. These
740 quantifications were done blind.
741 *Ligand receptor screen:* We quantified the number of L5s based on Elav expression in the
742 proximal lamina. Column number was identified by counting HRP-labelled photoreceptor axon
743 bundles. We quantified 30 optical slices (step size = 1μm) located centrally in the lamina.
744
745 *Ligand over-expression quantifications:*

746 We quantified the number of L-neuron types per column using Elav, Bsh and Slp2. We
747 quantified 30 optical slices (step size = 1μm) located centrally in the lamina. Column number
748 was identified by counting HRP-labelled photoreceptor axon bundles.
749
750 *Spi and Col4a1 Probe Intensity Quantifications:*
751 In Fiji-ImageJ we used the free hand selection tool to draw a region of interest (ROI) around the
752 $xg^O$ (marked by the *$xg^O$>CD8::GFP*). We then measured the mean fluorescence intensity of *spi*
753 and *Col4a1* transcripts labelled by HCR within each ROI. We quantified 30 optical slices (step
754 size = 1μm) located centrally in the lamina and then plotted the average for each optic lobe.
755
756 *Number of $xg^O$:*
757 We quantified the number of $xg^O$ (Figure S1Q) by manually counting the number of Repo
758 positive nuclei within LifeAct-GFP positive $xg^O$ per 40μm optical section in Fiji-ImageJ. We
759 used a step size of 1mm while acquiring the z-stacks and centred each 40μm optical section in
760 the middle of the lamina using photoreceptor axons (HRP), and the lobula plug (Dac expression)
761 as landmarks. Quantifications were performed blind.
762
763 *Length of $xg^O$ processes:*
764 We quantified the lengths of the fine glial processes that extend distally from the $xg^O$ towards the
765 lamina plexus (Figure S1O,P,R) by using the straight-line selection and measuring tools in Fiji-
766 ImageJ to measure $xg^O$ process lengths in a 10mm optical section centred in the middle of the
767 lamina. Quantifications were performed blind.
768
769 *Quantifications of nuclear to cytoplasmic dpMAPK mean fluorescence intensity:*
770 Using Fiji we manually drew regions of interest (ROIs) with the free hand selection tool around
771 the $xg^O$ nucleus (based on Repo) and LPCs in the most proximal row of the lamina (based on
772 Dac expression) and added these to the ROI manager. We then enlarged the ROIs
773 (Edit>Selection>Enlarge) by 3.00 pixel units to include the cytoplasm. We then used the XOR
774 function in the ROI Manager to only select the cytoplasm of the $xg^O$. We then measured the MFI
775 of dpMAPK in the nucleus and the cytoplasm of the $xg^O$ in 20 centrally located optical slices

776 (corresponding to 20μm) for each optic lobe. We plotted the nuclear:cytoplasmic ratios of
777 dpMAPK MFI in GraphPad Prism8.
778
779 *aos-lacZ intensity quantifications:*
780 Using Fiji we manually drew regions of interest around L5s (based on Slp2 + Bsh co-expression)
781 in each column. We then measured the mean fluorescence intensity of β-Gal in the ROIs. We
782 quantified 10 optical slices (step size = 1μm) for each optic lobe and plotted the average values
783 as a function of column (age).

784 **Figure 1: EGFR activity in the $xg^O$ is required for the differentiation of L5 neurons.**
785 **(A)** Schematic of the developing lamina. Photoreceptors (blue) drive lamina precursor cell (LPC;
786 purple) birth from neuroepithelial cells (NE; grey) and their assembly into columns of ~6 LPCs,
787 which differentiate into the L1-L5 neurons (yellow) following an invariant spatiotemporal
788 pattern. The 'extra' LPC is cleared by apoptosis (red X). Several glial types (magenta) associate
789 with the lamina.
790 **(B)** A cross-sectional view of an early pupal (0-5 hours after puparium formation; APF) optic
791 lobe where *hh-Gal4* drives *UAS-CD8::GFP* expression in photoreceptors (cyan). The pan-glial
792 driver *repo-QF2* drives *QUAS-m.Cherry* (magenta) in all glia. Elav (yellow) marks all neurons.
793 **(C)** A cross-sectional view of an optic lobe with pan-glial expression of CD8::GFP stained for
794 GFP (cyan), Dac (magenta), Elav (yellow) and Horseradish peroxidase (HRP; axons; white).
795 **(D)** Pan-glial expression of 2 copies of $EGFR^{DN}$ stained for Dac (magenta), Elav (yellow) and
796 HRP (white).
797 (**E)** $xg^O$-specific expression of CD8::GFP stained for GFP (cyan), Dac (magenta), Elav (yellow)
798 and HRP (white).
799 **(F)** $xg^O$-specific expression of 2 copies of $EGFR^{DN}$ and CD8::GFP stained for GFP (cyan), Dac
800 (magenta), Elav (yellow) and HRP (white). The number of Elav+ cells in proximal row (L5s)
801 decreased (empty arrowhead) relative to control (E).
802 **(G,H)** HRP (white) and L-neuron type specific markers Slp2 (cyan), Bsh (yellow) and Svp
803 (magenta) in **(G)** Control $xg^O>lacZ$ optic lobe and **(H)** $xg^O>2xEGFR^{DN}$. L2s and L3s express
804 Slp2; L1s express Slp2 and Svp; L4s express Bsh and L5s express Bsh and Slp2.
805 **(I)** Quantification of the number of L-neuron types per column for control and $xg^O>2xEGFR^{DN}$.
806 Only L5 neurons were decreased significantly ($P^{L5}<0.0001$; Mann-Whitney U test. Ns indicated
807 in parentheses. Boxes indicate the lower and upper quartiles; the whiskers represent the
808 minimum and maximum values; the line inside the box indicates the median). Scale Bar = 20μm.

809 **Figure 1- figure supplement 1: A Gal4 screen identifies $xg^O$ as the glial sub-type that**
810 **regulates L5 neuronal differentiation**
811 **(A)** Schematic of the developing lamina and associated glial types (green; labelled).
812 **(B)** A perineurial glia specific Gal4 drives expression of myr.GFP stained for GFP (cyan), Dac
813 (magenta) and HRP (white).
814 **(C)** Perineurial glia specific expression of $EGFR^{DN}$ stained for Elav (yellow) and HRP (white).
815 L5 differentiation was not affected.
816 **(D)** A subperineurial glia specific Gal4 drives expression of myr.GFP stained for GFP (cyan),
817 Dac (magenta) and HRP (white).
818 **(E)** Suberineurial glia specific expression of $EGFR^{DN}$ stained for Elav (yellow) and HRP (white).
819 L5 differentiation was not affected.
820 **(F)** A cortex glia specific Gal4 drives expression of myr.GFP stained for GFP (cyan), Dac
821 (magenta) and HRP (white).
822 **(G)** Cortex glia specific expression of $EGFR^{DN}$ stained for Elav (yellow) and HRP (white). L5
823 differentiation was not affected.
824 **(H)** An epithelial and marginal glia (eg+mg) specific Gal4 drives expression of myr.GFP stained
825 for GFP (cyan), Dac (magenta) and HRP (white).
826 **(I)** Epithelial and marginal glia specific expression of $EGFR^{DN}$ stained for Elav (yellow) and
827 HRP (white). L5 differentiation was not affected.
828 **(J)** A wrapping glia and $xg^O$ specific Gal4 drives expression of myr.GFP stained for GFP (cyan),
829 Dac (magenta) and HRP (white).
830 **(K)** Wrapping glia and $xg^O$ specific expression of $EGFR^{DN}$ stained for Elav (yellow) and HRP
831 (white). L1-L4 and L5 differentiation were disrupted as observed by the lack of Elav+ cells in
832 the lamina.
833 **(L)** A chiasm glia ($xg^{O\ and}\ xg^{inner)}$ specific Gal4 drives expression of myr.GFP stained for GFP
834 (cyan), Dac (magenta) and HRP (white).
835 **(M)** Chiasm glia specific expression of $EGFR^{DN}$ stained for Elav (yellow) and HRP (white). L1-
836 L4 differentiation proceeded normally but L5 differentiation was disrupted as observed by the
837 lack of Elav+ cells in the proximal lamina.
838 **(N)** $Gal80^{ts}$-restricted Gal4 expression in $xg^O$, driving $EGFR^{DN}$ during lamina development (See
839 Supporting File 1) stained for Dac (magenta), Elav (yellow) and HRP (white). L5 neurons were

840 dramatically reduced.

841 **(O,P)** LifeAct-GFP expression driven in $xg^O$ in **(O)** controls and **(P)** when 2 copies of $EGFR^{DN}$

842 are coexpressed. In both conditions, the fine processes from the $xg^O$ are present.

843 **(Q)** Quantification of $xg^O$ numbers in control *$xg^O$>LifeAct-GFP+2xlacZ* and *$xg^O$>LifeAct-GFP*

844 *+ $2xEGFR^{DN}$*. P>0.05; Mann-Whitney U test. Ns indicated in parentheses.

845 **(R)** Quantification of the length of $xg^O$ fine processes in control *$xg^O$>LifeAct-GFP+2xlacZ* and

846 *$xg^O$>LifeAct-GFP + $2xEGFR^{DN}$*. P>0.05; Unpaired t test. Ns indicated in parentheses.

847 **(S)** Wildtype adult optic lobe stained for Pdm3 (L5 marker) (Tan et al., 2015), Bruchpilot (Brp;

848 marks neuropils) and Elav (yellow).

849 **(T)** *$xg^O$>$2xEGFR^{DN}$* adult optic lobe stained for Pdm3 (L5 marker) (Tan et al., 2015), Bruchpilot

850 (Brp; marks neuropils) and Elav (yellow). Pdm3+ cells (L5s) are reduced dramatically.

851 Scale bar = 20µm. For all quantifications boxes indicate the lower and upper quartiles; the

852 whiskers represent the minimum and maximum values; the line inside the box indicates the

853 median).

854 **Figure 2: LPCs that fail to differentiate into L5s undergo apoptosis.**

855 **(A)** Control $xg^{O}>lacZ$ optic lobe stained for Dcp-1 (cyan), Elav (yellow) and HRP (white). Dcp-
856 1+ cells were always observed just distal to the most proximal row of cells (L5s).

857 **(B)** $xg^{O}>EGFR^{DN}$ stained for Dcp-1 (cyan), Dac (magenta) Elav (yellow) and HRP (white). Dcp-
858 1 positive cells were observed in the most proximal row of LPCs as well as the row just distal to
859 these.

860 **(C)** Quantification of the number of LPCs/column (*i.e.* Dac+ cells/column) for control and
861 $xg^{O}>EGFR^{DN}$. P*<0.05, P****<0.0002; Mann-Whitney U test. Ns indicated in parentheses.

862 **(D)** Quantification of the number of Dcp-1 positive cells in (A) compared to (B). P***<0.0005,
863 Mann-Whitney U test. Ns indicated in parentheses.

864 Boxes indicate the lower and upper quartiles; the whiskers represent the minimum and maximum
865 values; the line inside the box indicates the median). Scale bar = 20μm.

866 **Figure 3: $Xg^O$ secrete multiple ligands to induce L5 neuronal differentiation in response to**
867 **EGF from photoreceptors.**
868 **(A)** GMR-Gal4 driven CD8::GFP expression in photoreceptors in a *rho3*$^{PLLb}$ background stained
869 for GFP (white), Dac (magenta), Elav (yellow). Few proximal Elav+ cells (L5s) were recovered
870 in older columns only as previously published (Fernandes et al., 2017).
871 **(B)** GMR-Gal4 driven Rho3 and CD8::GFP in a *rho3*$^{PLLb}$ background stained for GFP (white),
872 Dac (magenta), Elav (yellow) showed that L5 neuronal differentiation was rescued (Elav+ cells
873 in the proximal lamina).
874 **(C)** Quantifications for number of L5 neurons/column in (A) and (B) compared to *rho3*$^{PLLb}$
875 heterozygotes *(rho3*/+). P****<0.0001, one-way ANOVA with Dunn's multiple comparisons
876 test. Ns indicated in parentheses.
877 **(D,E)** Control *xg*$^{O}$*>GFP* optic lobes stained for **(D)** Dac (magenta), Elav (yellow) and HRP
878 (white) or **(E)** HRP (white) and L-neuron specific markers Slp2 (cyan) and Bsh (yellow).
879 **(F,G)** Gal4 titration control *xg*$^{O}$*>GFP+EGFR*$^{DN}$ stained for **(F)** Dac (magenta), Elav (yellow)
880 and HRP (white) or **(G)** HRP (white) and L-neuron specific markers Slp2 (cyan) and Bsh
881 (yellow).
882 **(H,I)** Wild-type Spi ($Spi^{wt}$) co-expression with $EGFR^{DN}$ specifically in $xg^O$ stained for **(H)** Elav
883 (yellow) and HRP (white) or **(I)** HRP (white) and L-neuron specific markers Slp2 (cyan) and
884 Bsh (yellow).
885 **(J,K)** Col4a1 co-expression with $EGFR^{DN}$ specifically in $xg^O$ stained for **(J)** Elav (yellow) and
886 HRP (white) or **(K)** HRP (white) and L-neuron specific markers Slp2 (cyan) and Bsh (yellow).
887 **(L,M)** Gal4 titration control *xg*$^{O}$*>EGFR*$^{DN}$*+2xlacZ* stained for **(L)** Elav (yellow) and HRP
888 (white) or **(M)** HRP (white), Slp2 (cyan) and Bsh (yellow).
889 **(N,O)** Wild-type $Spi^{wt}$ and Col4a1 co-expression with $EGFR^{DN}$ specifically in $xg^O$. **(N)** stained
890 for Elav (yellow) and HRP (white) or **(O)** HRP (white) and L-neuron specific markers Slp2
891 (cyan) and Bsh (yellow).
892 **(P)** Quantification of the number of L5s/column for the genotypes indicated compared to the
893 appropriate titration control. For *pntP1*, *spi*$^{wt}$, and *Col4a1* co-expression with $EGFR^{DN}$ the
894 titration control is *xg*$^{O}$*>EGFR*$^{DN}$*+GFP* (P**<0.005, P$^{***}$<0.0005; P$^{****}$<0.0001; one-way
895 ANOVA with Dunn's multiple comparisons test. Ns indicated in parentheses). For *spi*$^{wt}$ and
896 *Col4a1* simultaneous co-expression with $EGFR^{DN}$ the titration control is *xg*$^{O}$*>EGFR*$^{DN}$*+2xLacZ*

897 (P****<0.0001, Mann-Whitney U Test. Ns indicated in parentheses).

898 **(Q,R)** Optic lobes stained for Slp2 and Bsh when $xg^{O}$ overexpress **(Q)** *$spi^{wt}$* or **(R)** *Col4a1*.

899 **(S)** Quantification of the number of L-neuron types/column in (Q) and (R) compared to controls,

900 *$xg^{O}$>lacZ*. (P*<0.05; P**<0.005; P***<0.001; one-way ANOVA with multiple comparisons

901 test).

902 **(T, U, V)** Optic lobes stained for Slp2, Bsh and HRP when $xg^{O}$ co-express Dcr-2 with **(T)**

903 $spi^{RNAi}$, **(U)** $Col4a1^{RNAi}$ and **(V)** $Spi^{RNAi}$ and $Col4a1^{RNAi}$ simultaneously.

904 **(W)** Quantifications of the number of L5s/column for genotypes indicated compared to the

905 titration control *$xg^{O}$>Dcr-2+lacZ* (P*<0.05, P****<0.0001, one-way ANOVA with Dunn's

906 multiple comparisons test.

907 Scale bar = 20µm. For all quantifications boxes indicate the lower and upper quartiles; the

908 whiskers represent the minimum and maximum values; the line inside the box indicates the

909 median).

910 **Figure 3- figure supplement 1: Multiple $xg^O$ secreted ligands activate MAPK signalling to**
911 **drive L5 neuronal differentiation**
912 **(A,B)** Optic lobes stained for Elav (yellow), Repo (magenta) and dpMAPK (cyan) in **(A)**
913 *$xg^O$>lacZ* controls and **(B)** with $EGFR^{DN}$ and lacZ expressed in $xg^O$. dpMAPK levels decreased
914 in the $xg^O$ (indicated by asterisk) and in cells in the proximal row of the lamina (indicated by
915 arrowhead) when compared with *$xg^O$>lacZ* controls.
916 **(C)** Quantification of the number of L5s/column (based on Elav expression) when different
917 ligands that can activate MAPK signalling were co-expressed with $EGFR^{DN}$ in the $xg^O$.
918 (P*<0.05; P**<0.01; P***<0.0005; P****<0.0001; one-way ANOVA with Dunn's multiple
919 comparison test. Ns indicated in parentheses).
920 **(D)** *bnl>CD8::GFP* showed GFP (cyan) expression in all cells in the optic lobe; HRP (white).
921 **(E)** *ths>CD8::GFP* showed GFP (cyan) expression in photoreceptors; HRP (white).
922 **(F)** *Collagen>CD8::GFP* drove GFP (cyan) expression in $xg^O$ (arrowhead); Elav (yellow).
923 **(G)** *$spi^{NP0289}$>CD8::GFP* drove GFP (cyan) expression in $xg^O$ (arrowhead); Elav (yellow).
924 **(H, I)** *$xg^O$>GFP* lobes stained for GFP (cyan) and **(H)** *spi* mRNA (magenta) and **(I)** *Col4a1*
925 mRNA (magenta) by *in situ* hybridisation chain reaction (HCR).
926 **(J)** *$xg^O$>$EGFR^{DN}$+s.spi* lobes stained for Elav (yellow), Repo (magenta) and dpMAPK (cyan).
927 Inset shows a magnified view of the $xg^O$ nucleus.
928 **(K)** Quantifications of nuclear:cytoplasmic ratios of dpMAPK MFI in the $xg^O$ in indicated
929 genotypes (P<0.0005, one-way ANOVA with Dunn's multiple comparisons test. Ns indicated in
930 parentheses)
931 **(L)** *spi* mRNA (magenta) detected by HCR in *$xg^O$>GFP+2x$EGFR^{DN}$* lobes.
932 **(M)** Quantification of *spi* MFI (arbitrary units) for (H and L). (P<0.05; Mann-Whitney U test.)
933 **(N)** *Col4a1* mRNA (magenta) detected by HCR in *$xg^O$>GFP+2x$EGFR^{DN}$* lobes.
934 **(O)** Quantification of *Col4a1* MFI (arbitrary units) for (I and N) (P<0.005; Mann-Whitney U
935 test). **(P)** *Ddr>lacZ* showed β-Galactosidase (β-Gal; cyan) expression in the lamina; HRP
936 (white).
937 **(Q)** *Ddr* mRNA (magenta) detected by HCR in w*ild-type* lobes; DAPI (white).
938 **(R,S)** Lobes stained for Dac (magenta), Elav (yellow) and dpMAPK (cyan) when **(R)** $Spi^{wt}$ is
939 coexpressed with $EGFR^{DN}$ in $xg^O$ or **(S)** Col4a1 is coexpressed with $EGFR^{DN}$ in $xg^O$.
940 Arrowheads indicate Elav+ cells in the most proximal row.

941 **(T)** Quantifications of nuclear:cytoplasmic ratios of dpMAPK MFI in the most proximal row of
942 LPCs in indicated genotypes (P**<0.005. P****<0.0001; one-way ANOVA with Dunn's
943 multiple comparisons test).
944 Scale bar = 20μm. For all quantifications boxes indicate the lower and upper quartiles; the
945 whiskers represent the minimum and maximum values; the line inside the box indicates the
946 median).

947 **Figure 3- figure supplement 2: Spi and Col4a1 from $xg^{O}$ promote cell survival in proximal**
948 **LPCs.**
949 **(A)** *$xg^{O}$>lacZ* lobes stained for Dcp-1 (cyan), Dac (magenta), Elav (yellow) and HRP (white).
950 Dcp-1 positive cells (indicated by arrowhead) were located between L4s and L5s and
951 corresponds to 'extra' LPCs which undergo apoptosis.
952 **(B)** *$xg^{O}$>$Spi^{RNAi}$+$Col4a^{RNAi}$+ Dcr-2* lobes stained for Dcp-1 (cyan), Dac (magenta), Elav
953 (yellow) and HRP (white). Dcp-1 positive cells were observed in the proximal row of L5s
954 (indicated by arrowhead) which were never observed in controls.

955 **Figure 4: The 'extra' LPCs are specified as L5s**

956 **(A)** Wild-type optic lobes stained for Dac (magenta), HRP (white), Elav (yellow) and cleaved
957 Dcp-1 (cyan).

958 **(B)** Wild-type optic lobes stained for HRP (white) and L-neuron type specific markers Slp2
959 (cyan) and Bsh (yellow).

960 **(C, D)** Optic lobes with lamina-specific overexpression of PntP1 stained as in (A) and (B),
961 respectively. **(C)** Fewer Dcp-1 positive cells were recovered compared with controls. **(D)**
962 Roughly two rows of Slp2 and Bsh co-expressing cells (L5s) were recovered (arrow heads).

963 **(E)** Quantification of the number of Dcp-1 positive cells in (B) compared with control
964 *Lamina$^{ts}$>lacZ* (Figure 4- figure supplement 1A) ($P<0.0001$; Mann-Whitney U test).

965 **(F)** Quantification of the number of L-neuron types per column based on Slp2 and Bsh
966 expression from column 7 onwards shows an increase in the number of L5s/column in
967 *Lamina$^{ts}$>PntP1* compared with controls; $P<0.0001$; Mann-Whitney U test.

968 **(G)** Same as (F) but normalised to the mean of the control. The number of L5s/column in
969 *Lamina$^{ts}$>PntP1* increase ~1.2 fold relative to controls; $P <0.0001$; Mann-Whitney U Test. Ns
970 indicated in parentheses.

971 Scale bar = 20µm. For all quantifications boxes indicate the lower and upper quartiles; the
972 whiskers represent the minimum and maximum values; the line inside the box indicates the
973 median).

974 **Figure 4- figure Supplement 1: Hyperactivating MAPK in the lamina drives ectopic L5**
975 **differentiation**
976 **(A,B)** Control *Lamina$^{ts}$>lacZ* optic lobes stained for **(A)** Dac (magenta), HRP (white) and Elav
977 (yellow), and **(B)** and L-neuron type specific markers Slp2 (cyan) and Bsh (yellow).
978 **(C,D)** *Lamina$^{ts}$>MAPK$^{ACT}$* optic lobes stained for **(C)** Dac (magenta), HRP (white) and Elav
979 (yellow), and **(D)** L-neuron type specific markers Slp2 (cyan) and Bsh (yellow). Ectopic Slp2
980 and Bsh co-expressing cells (L5s) were observed (arrowheads).
981 **(E)** Quantification of the number of Elav+ cells per lamina column as a function of column
982 number (age) in wildtype animals. Columns were fully differentiated (5 Elav+ cells) by column
983 7. Boxes indicate the lower and upper quartiles; the whiskers represent the minimum and
984 maximum values; the line inside the box indicates the median). Scale bar = 20μm.

985 **Figure 5: Newly-induced L5 neurons secrete Aos to limit differentiation signals from $xg^{O}$.**
986 **(A)** *Dronc*$^{I24}$ optic lobes stained for Dcp-1 (cyan), Dac (magenta), Elav (yellow) and HRP
987 (white). No Dcp-1 positive cells were recovered and Dac positive cells between L1-L4s and L5s
988 persisted into the oldest columns (asterisk).
989 **(B)** *Dronc*$^{I24}$ optic lobes stained for L-neuron type specific markers Slp2 (cyan) and Bsh
990 (yellow). A space (negative for both markers; asterisk) was present between L4s and L5s.
991 **(C)** Quantifications for number of L5s/column in *Dronc*$^{I24}$ optic lobes compared to controls
992 (*Dronc*$^{I24}$/+) (P>0.05, Mann-Whitney U test. Ns indicated in parentheses).
993 **(D,E)** *aos-lacZ* expression in the lamina with **(D)** β-Gal (cyan), Repo (magenta), Elav (yellow),
994 HRP (white) and with **(E)** β-Gal (magenta) and L-neuron type specific markers Slp2 (cyan), Bsh
995 (yellow) as well as HRP (white).
996 **(F)** An L5-specific Gal4 was used to drive expression of *Dcr-2* and *lacZ* in control lobes stained
997 for Slp2 (cyan), Bsh (yellow) and HRP (white).
998 **(G)** Optic lobes stained for HRP (white), Slp2 (cyan) and Bsh (yellow) when *Dcr-2* and *aos*$^{RNAi}$
999 were expressed in developing L5 neurons specifically, which led to an increase in the number of
1000 Slp2 and Bsh co-expressing cells (L5s; asterisks).
1001 **(H)** Quantification of the number of L5s/column for (F) and (G). P***<0.0005; Mann-Whitney
1002 U test. Ns indicated in parentheses.
1003 For all quantifications boxes indicate the lower and upper quartiles; the whiskers represent the
1004 minimum and maximum values; the line inside the box indicates the median). Scale bar = 20μm.

1005 **Figure 5-figure supplement 1: Aos expression is delayed in younger L5s.**

1006 **(A)** An L5 specific driver was used to drive the expression of GFP (magenta) in the lamina; HRP
1007 (white) and L-neuron type specific markers Slp2 (cyan) and Bsh (yellow).

1008 **(B)** β-Gal MFI quantifications in the proximal row of L5s as a function of column number (age)
1009 in *aos-lacZ* lobes. β-Gal MFI is low in young columns and increases in older columns (from
1010 column 5). Boxes indicate the lower and upper quartiles; the whiskers represent the minimum
1011 and maximum values; the line inside the box indicates the median). Scale bar = 20μm.

1012 **Figure 6: Summary schematic of neuronal differentiation in the lamina**

1013 In our model of lamina neuronal differentiation, lamina precursor cells are prepatterned with
1014 unique identities based on their positions within a column, such that the two most proximal cells
1015 are specified with L5 identity. EGF from photoreceptors activates EGFR signalling in wrapping
1016 glia, which induce L1-L4 differentiation, and in $xg^{O}$, which induce L5 differentiation. Only a
1017 subset of the LPCs specified as L5s differentiate (*i.e.* those in the proximal row). We propose
1018 that this selective neuronal induction of L5s is due to tissue architecture and feedback from the
1019 newly born L5s, which limit available EGF (Spi) by secreting the antagonist Aos.

1020 **Supplementary File 1: Table summarising the results from the glial-Gal4 screen (Figure 1**
1021 **B,C, Figure 1- figure supplement 1B-N) to identify the glial type that regulates L5**
1022 **development.**
1023
1024
1025 **Supplementary File 2: Table listing all genotypes and experimental conditions used by**
1026 **figure panel.** (Note that only female genotypes are listed though both sexes were included in our
1027 analyses)
1028
1029
1030 **Supporting zip document 1: Excel file containing all the probe sequences used for *in situ***
1031 **hybridisation chain reaction in this study**

# Figure 1

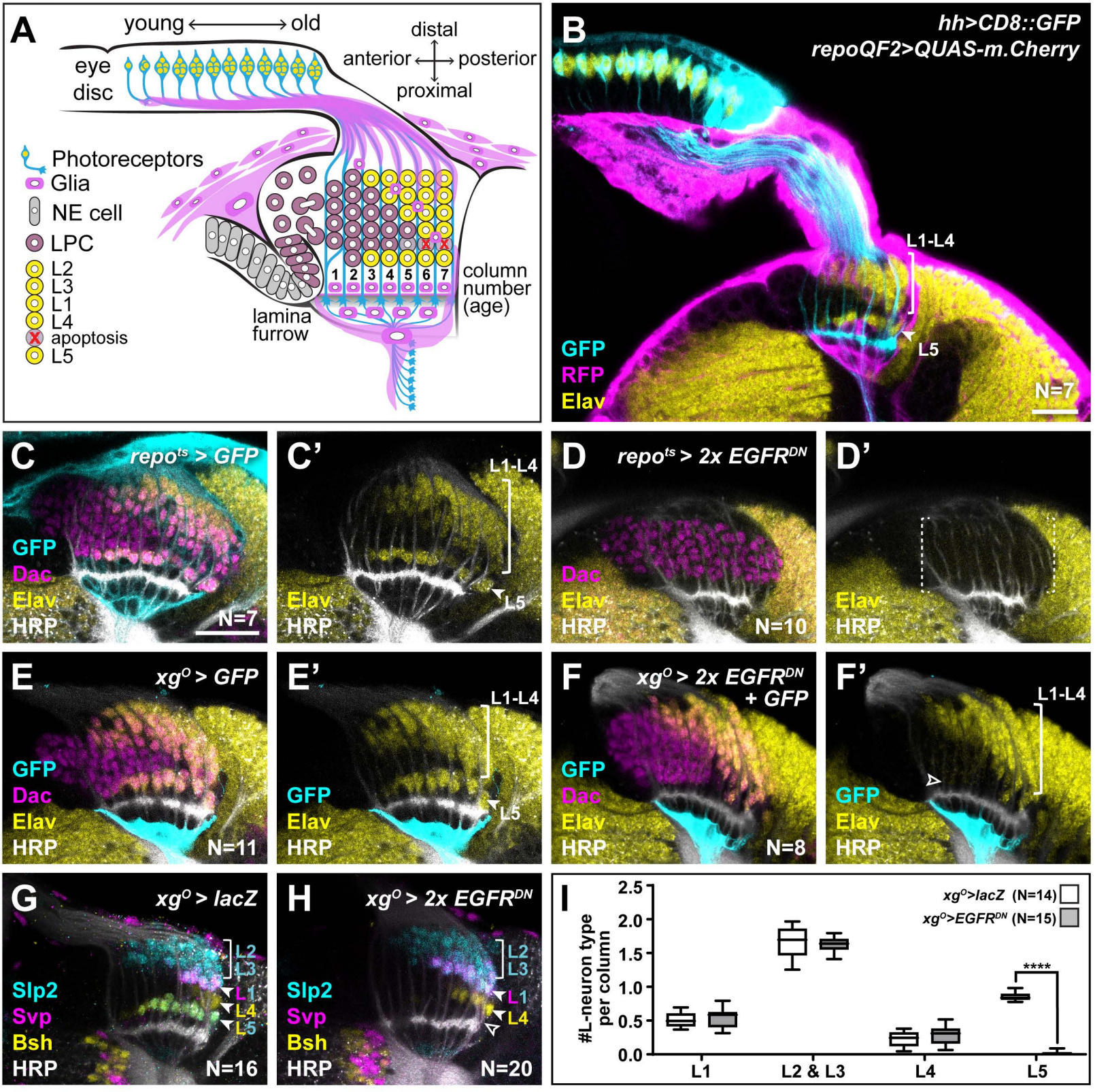
A
young ⟷ old
distal
anterior ⟷ posterior
proximal
eye disc
Photoreceptors
Glia
NE cell
LPC
L2
L3
L1
L4
apoptosis
L5
1 2 3 4 5 6 7
column number (age)
lamina furrow
B
hh>CD8::GFP
repoQF2>QUAS-m.Cherry
L1-L4
L5
GFP
RFP
Elav
N=7
C
repo^ts > GFP
GFP
Dac
Elav
HRP
N=7
C'
L1-L4
L5
Elav
HRP
D
repo^ts > 2x EGFR^DN
Dac
Elav
HRP
N=10
D'
Elav
HRP
E
xg^O > GFP
GFP
Dac
Elav
HRP
N=11
E'
L1-L4
L5
GFP
Elav
HRP
F
xg^O > 2x EGFR^DN + GFP
GFP
Dac
Elav
HRP
N=8
F'
L1-L4
GFP
Elav
HRP
G
xg^O > lacZ
L2
L3
L1
L4
L5
Slp2
Svp
Bsh
HRP
N=16
H
xg^O > 2x EGFR^DN
L2
L3
L1
L4
Slp2
Svp
Bsh
HRP
N=20
I
xg^O>lacZ (N=14)
xg^O>EGFR^DN (N=15)
#L-neuron type per column
2.5
2.0
1.5
1.0
0.5
0.0
****
L1
L2 & L3
L4
L5

# Figure 1- Figure supplement 1

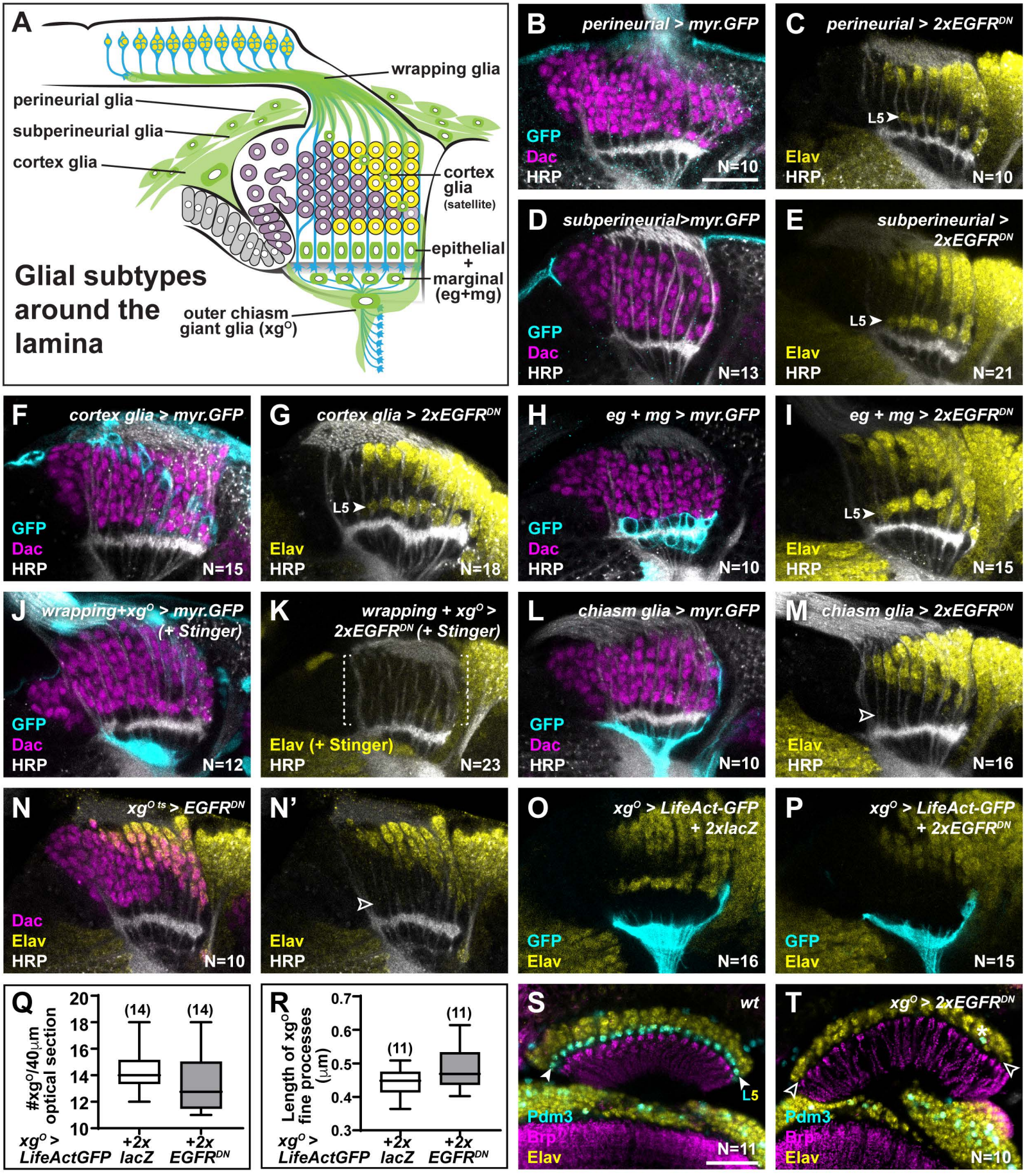

Figure 2

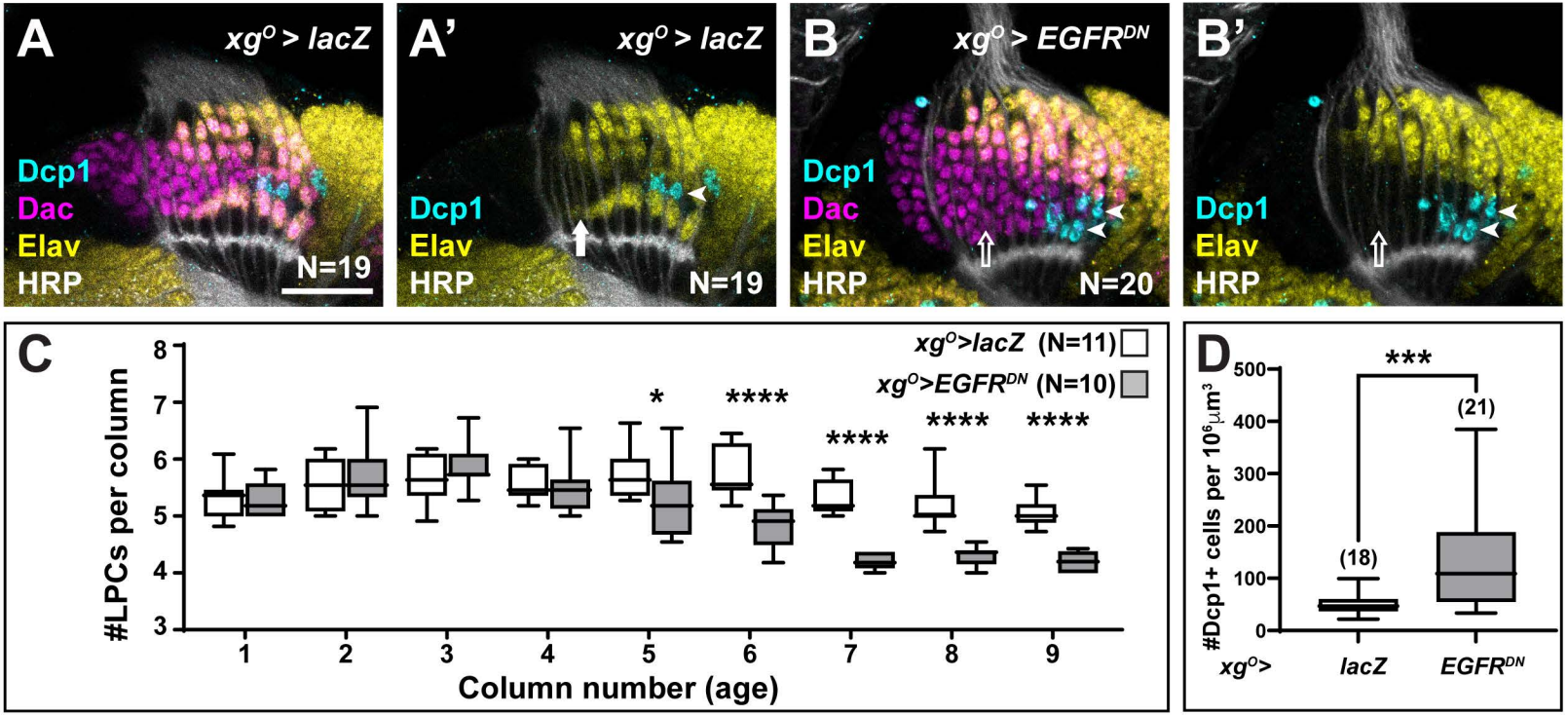
A
xg^O > lacZ
Dcp1
Dac
Elav
HRP
N=19
A'
xg^O > lacZ
Dcp1
Elav
HRP
N=19
B
xg^O > EGFR^DN
Dcp1
Dac
Elav
HRP
N=20
B'
Dcp1
Elav
HRP
C
xg^O>lacZ (N=11)
xg^O>EGFR^DN (N=10)
#LPCs per column
Column number (age)
*
****
****
****
****
D
#Dcp1+ cells per 10^6 µm^3
***
(18)
(21)
xg^O>
lacZ
EGFR^DN

Figure 3

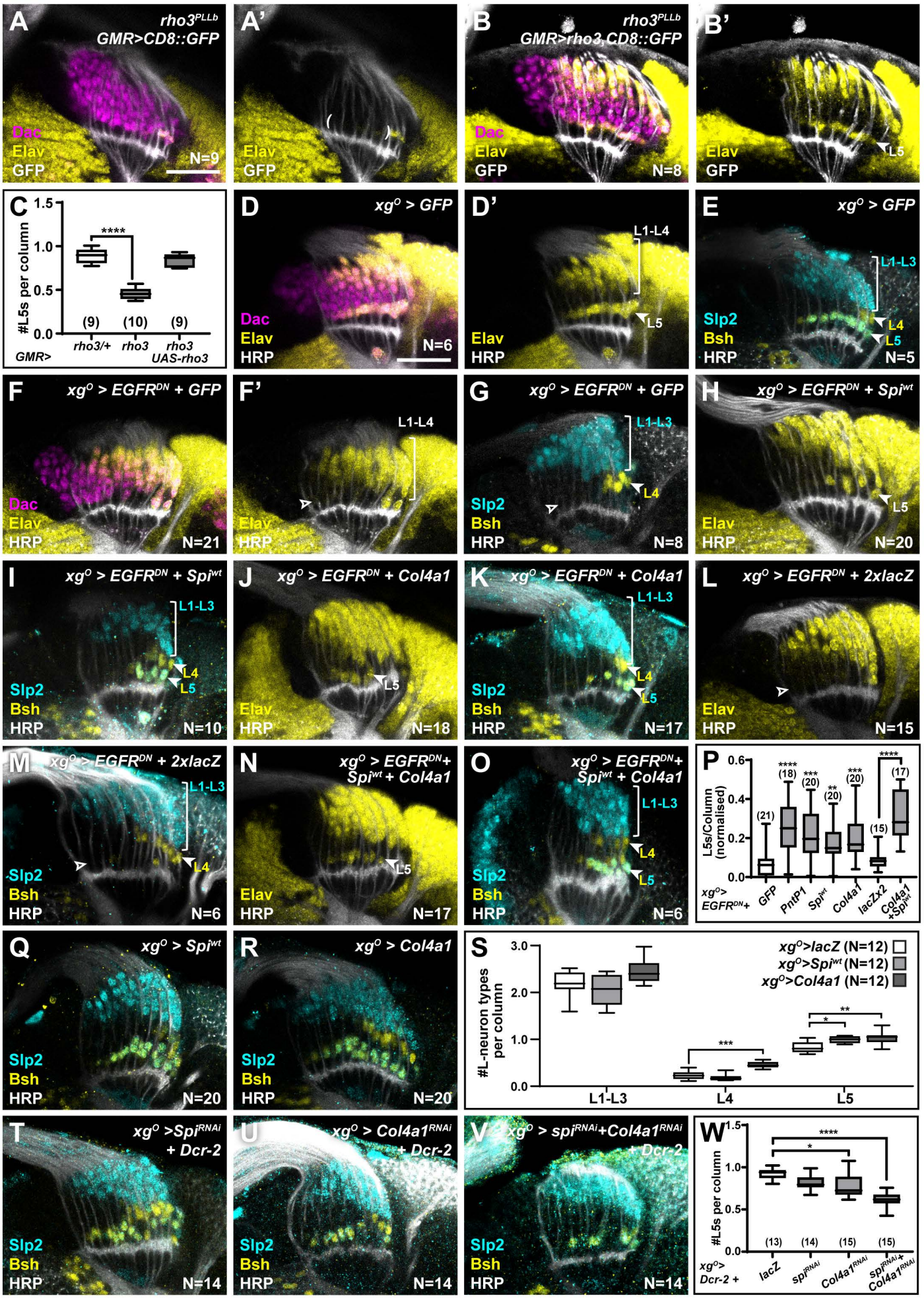
A
rho3PLLb
GMR>CD8::GFP
Dac
Elav
GFP
N=9
A'
Elav
GFP
B
rho3PLLb
GMR>rho3,CD8::GFP
Dac
Elav
GFP
N=8
B'
Elav
GFP
L5
C
#L5s per column
1.5
1.0
0.5
0.0
****
(9)
(10)
(9)
rho3/+
rho3
rho3
UAS-rho3
GMR>
D
xgO > GFP
Dac
Elav
HRP
N=6
D'
L1-L4
L5
Elav
HRP
E
xgO > GFP
L1-L3
Slp2
Bsh
HRP
L4
L5
N=5
F
xgO > EGFRDN + GFP
Dac
Elav
HRP
N=21
F'
L1-L4
Elav
HRP
G
xgO > EGFRDN + GFP
L1-L3
L4
Slp2
Bsh
HRP
N=8
H
xgO > EGFRDN + Spiwt
L5
Elav
HRP
N=20
I
xgO > EGFRDN + Spiwt
L1-L3
L4
L5
Slp2
Bsh
HRP
N=10
J
xgO > EGFRDN + Col4a1
L5
Elav
HRP
N=18
K
xgO > EGFRDN + Col4a1
L1-L3
L4
L5
Slp2
Bsh
HRP
N=17
L
xgO > EGFRDN + 2xlacZ
Elav
HRP
N=15
M
xgO > EGFRDN + 2xlacZ
L1-L3
L4
Slp2
Bsh
HRP
N=6
N
xgO > EGFRDN+
Spiwt + Col4a1
L5
Elav
HRP
N=17
O
xgO > EGFRDN+
Spiwt + Col4a1
L1-L3
L4
L5
Slp2
Bsh
HRP
N=6
P
L5s/Column
(normalised)
0.6
0.4
0.2
0.0
(21)
****
(18)
***
(20)
**
(20)
***
(20)
(15)
****
(17)
xgO>
EGFRDN+
GFP
PntP1
Spiwt
Col4a1
lacZx2
Col4a1
+Spiwt
Q
xgO > Spiwt
Slp2
Bsh
HRP
N=20
R
xgO > Col4a1
Slp2
Bsh
HRP
N=20
S
#L-neuron types
per column
3.0
2.0
1.0
0.0
xgO>lacZ (N=12)
xgO>Spiwt (N=12)
xgO>Col4a1 (N=12)
***
*
**
L1-L3
L4
L5
T
xgO >SpiRNAi
+ Dcr-2
Slp2
Bsh
HRP
N=14
U
xgO > Col4a1RNAi
+ Dcr-2
Slp2
Bsh
HRP
N=14
V
xgO > spiRNAi+Col4a1RNAi
+ Dcr-2
Slp2
Bsh
HRP
N=14
W
#L5s per column
1.5
1.0
0.5
0.0
****
*
(13)
(14)
(15)
(15)
xgO>
Dcr-2 +
lacZ
spiRNAi
Col4a1RNAi
spiRNAi+
Col4a1RNAi

# Figure 3- Figure supplement 1

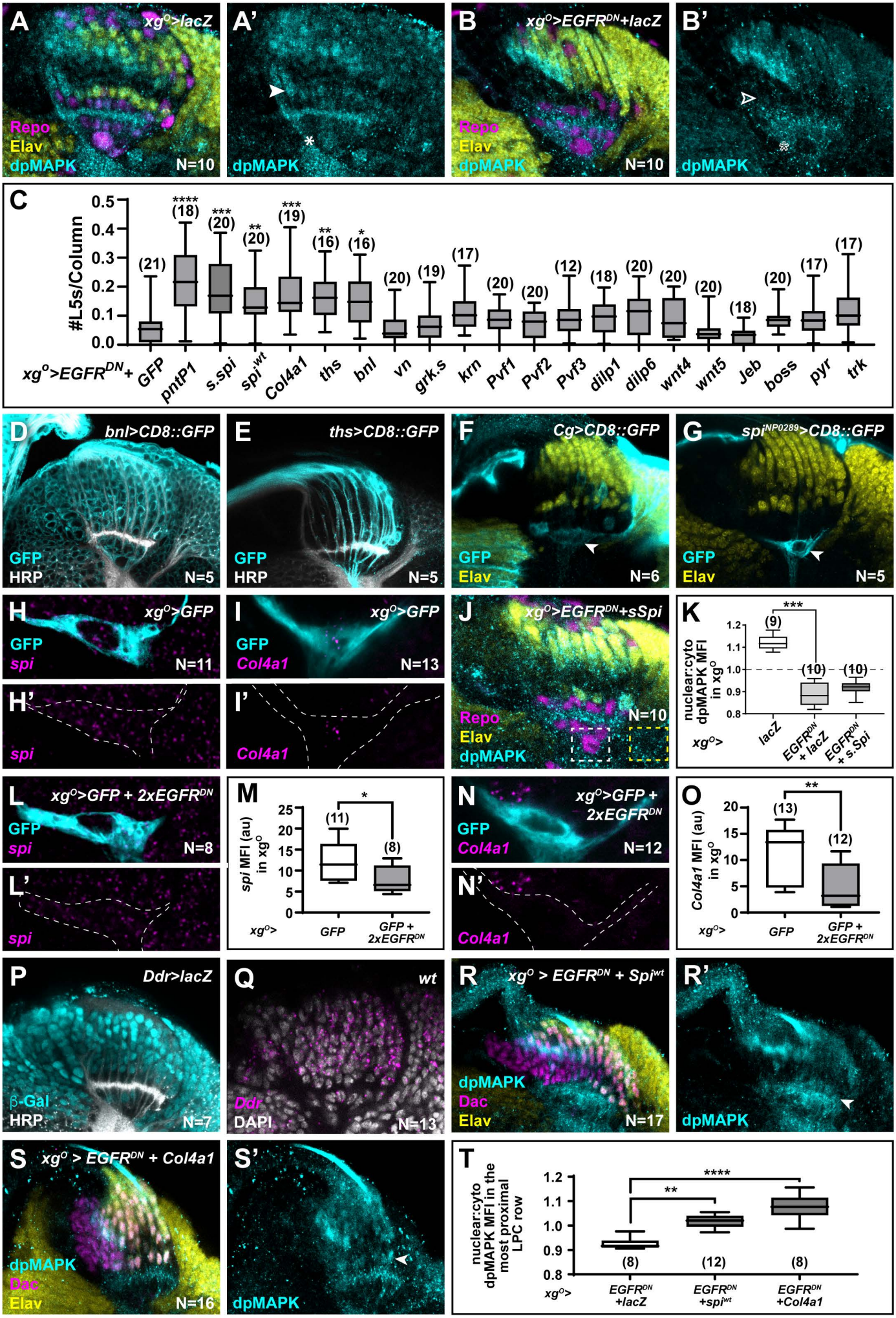

# Figure 3- Figure supplement 2

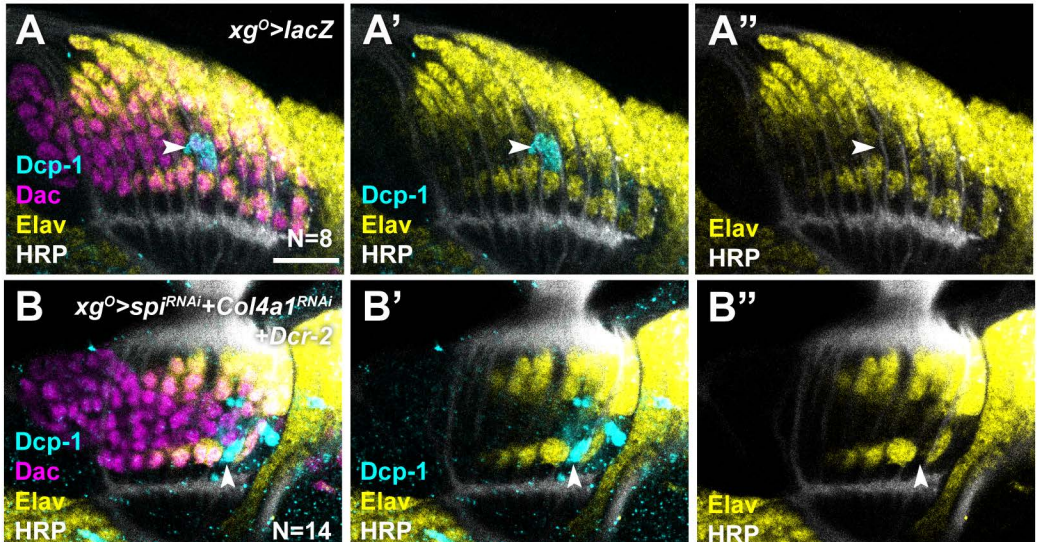

# Figure 4

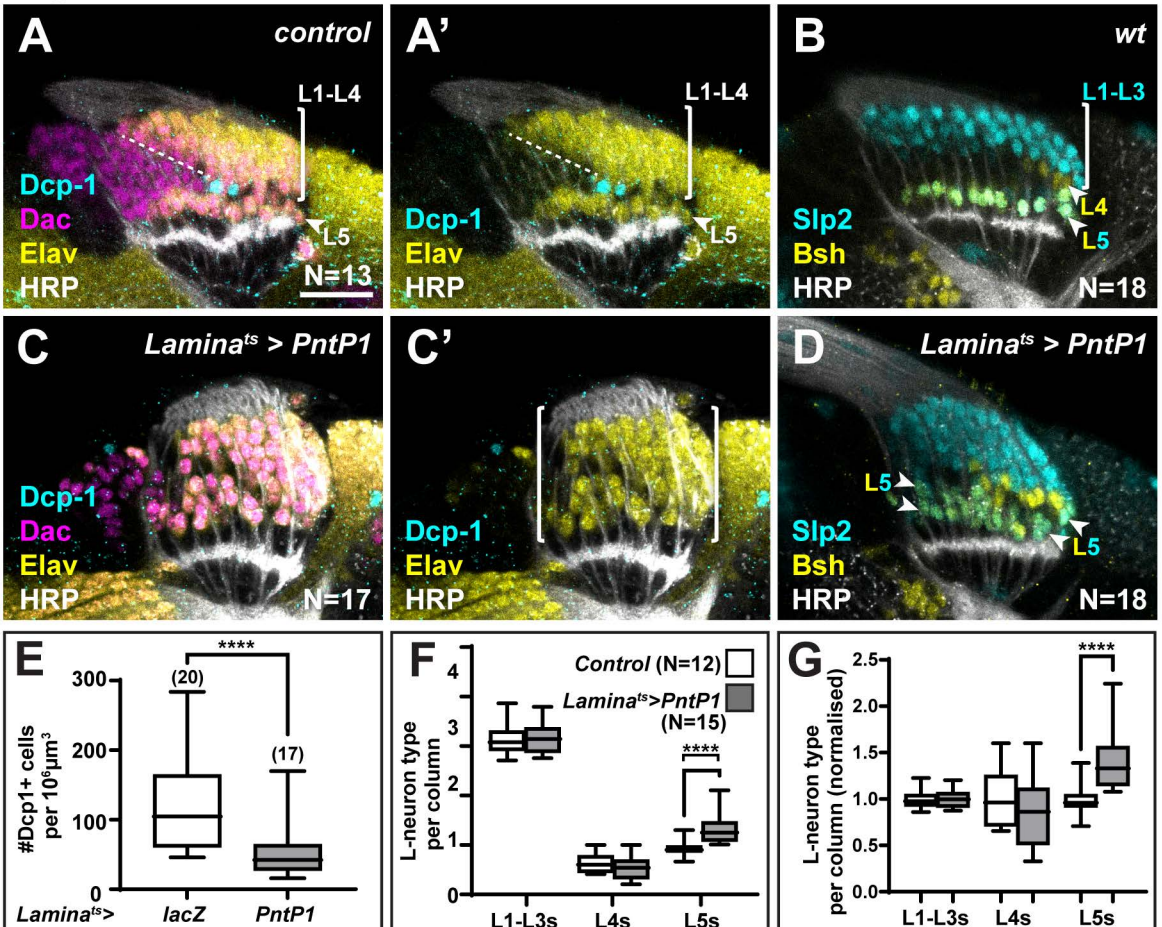
A
control
L1-L4
Dcp-1
Dac
Elav
HRP
L5
N=13
A'
L1-L4
Dcp-1
Elav
HRP
L5
B
wt
L1-L3
Slp2
Bsh
HRP
L4
L5
N=18
C
Lamina^ts > PntP1
Dcp-1
Dac
Elav
HRP
N=17
C'
Dcp-1
Elav
HRP
D
Lamina^ts > PntP1
L5
Slp2
Bsh
HRP
L5
N=18
E
****
(20)
(17)
#Dcp1+ cells per 10^6 µm^3
300
200
100
0
Lamina^ts>
lacZ
PntP1
F
Control (N=12)
Lamina^ts>PntP1 (N=15)
****
L-neuron type per column
4
3
2
1
0
L1-L3s
L4s
L5s
G
****
L-neuron type per column (normalised)
2.5
2.0
1.5
1.0
0.5
0.0
L1-L3s
L4s
L5s

Figure 4 - figure supplement 1

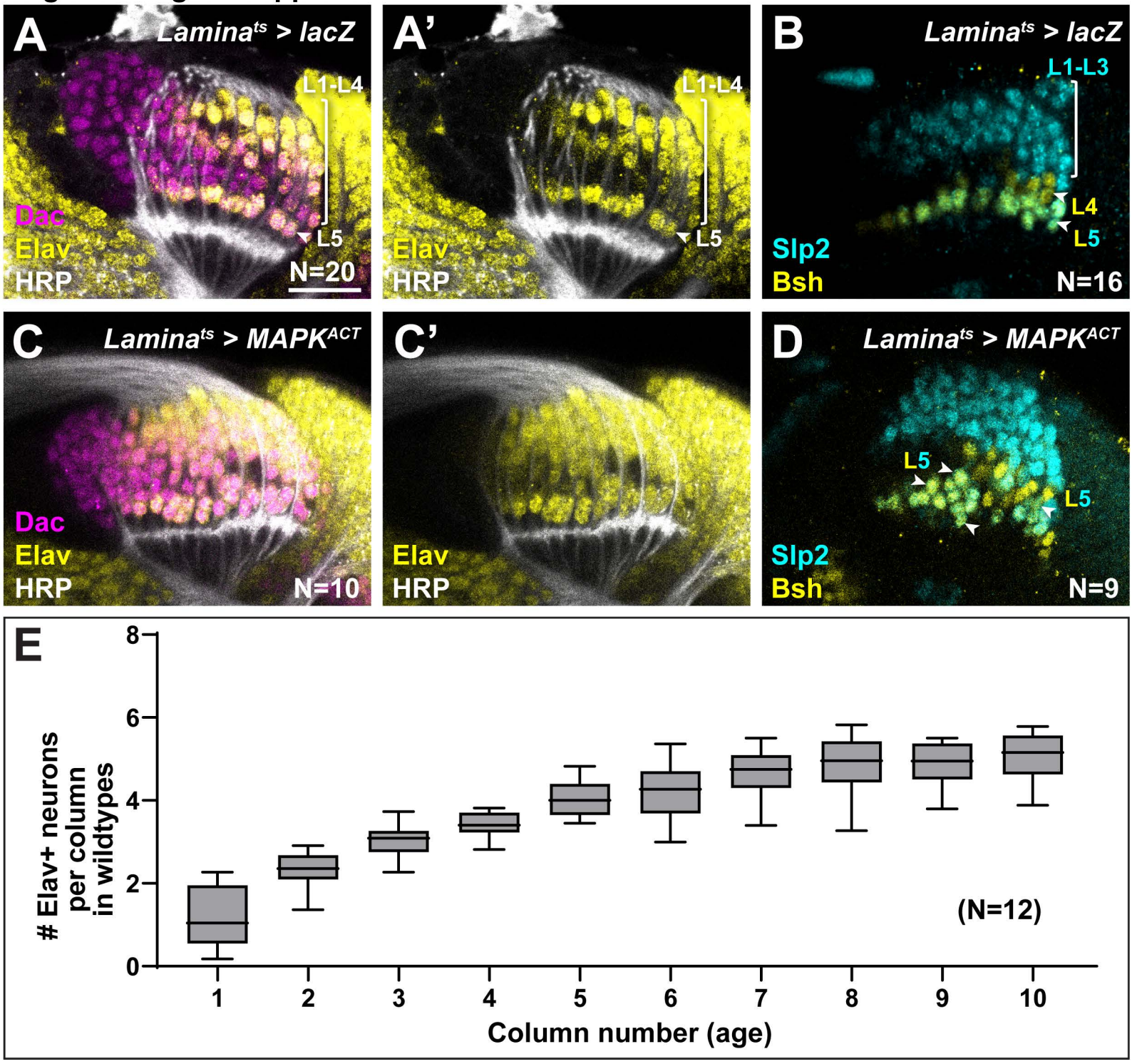

# Figure 5

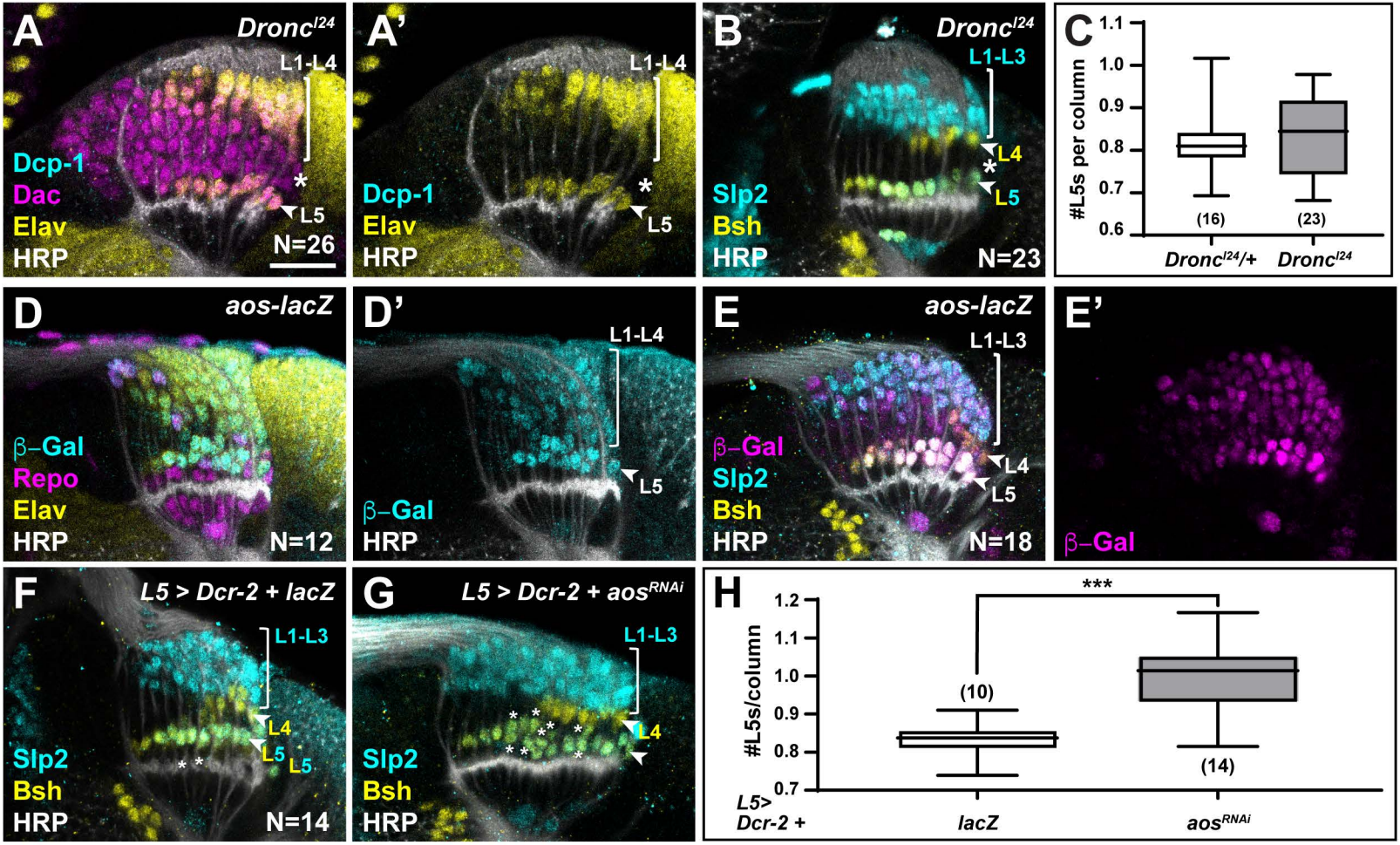
A
Dronc^I24
L1-L4
Dcp-1
Dac
Elav
HRP
L5
N=26
A'
L1-L4
Dcp-1
Elav
HRP
L5
B
Dronc^I24
L1-L3
L4
L5
Slp2
Bsh
HRP
N=23
C
#L5s per column
1.1
1.0
0.9
0.8
0.7
0.6
(16)
(23)
Dronc^I24/+
Dronc^I24
D
aos-lacZ
β-Gal
Repo
Elav
HRP
N=12
D'
L1-L4
L5
β-Gal
HRP
E
aos-lacZ
L1-L3
L4
L5
β-Gal
Slp2
Bsh
HRP
N=18
E'
β-Gal
F
L5 > Dcr-2 + lacZ
L1-L3
L4
L5
L5
Slp2
Bsh
HRP
N=14
G
L5 > Dcr-2 + aos^RNAi
L1-L3
L4
Slp2
Bsh
HRP
H
***
#L5s/column
1.2
1.1
1.0
0.9
0.8
0.7
(10)
(14)
L5>
Dcr-2 +
lacZ
aos^RNAi

# Figure 5 - Figure supplement 1

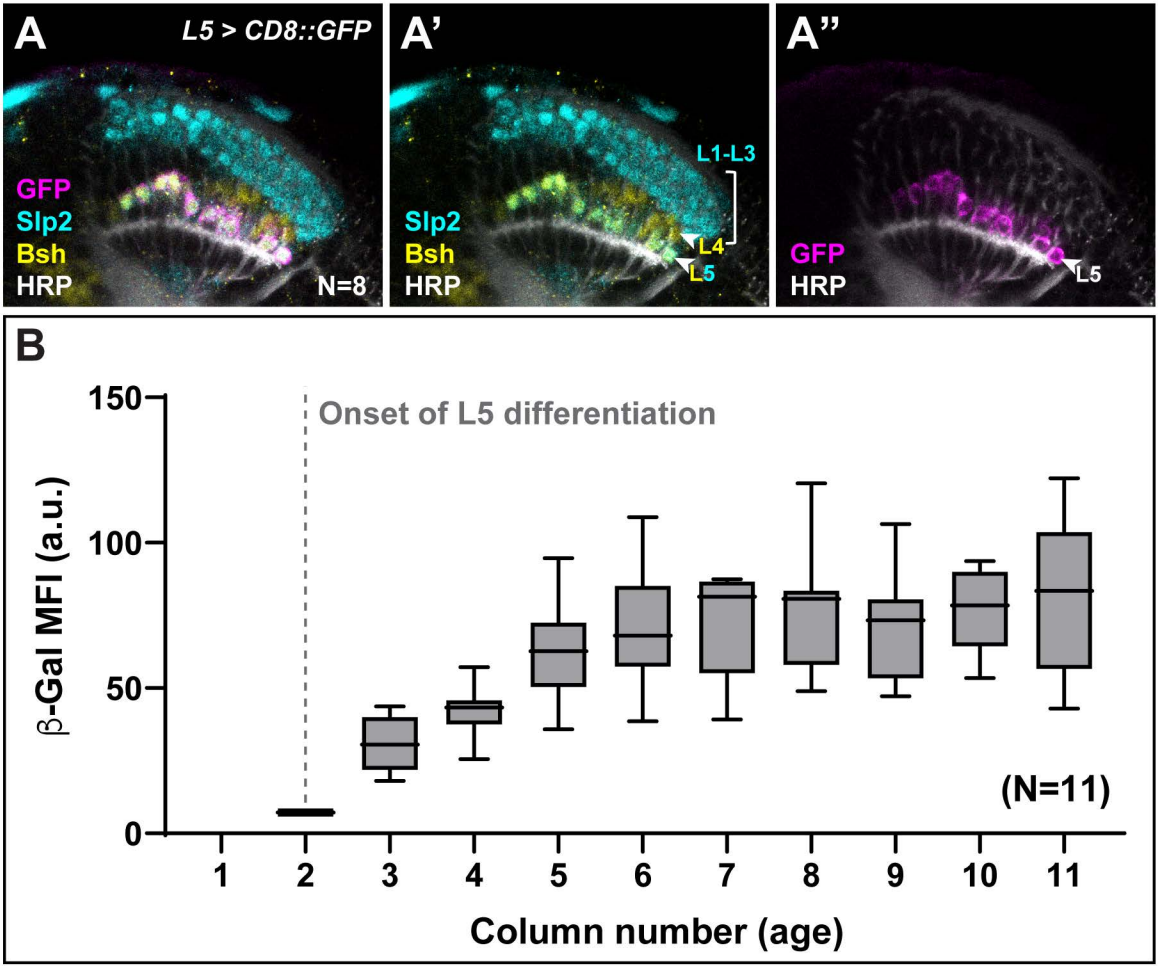

Figure 6

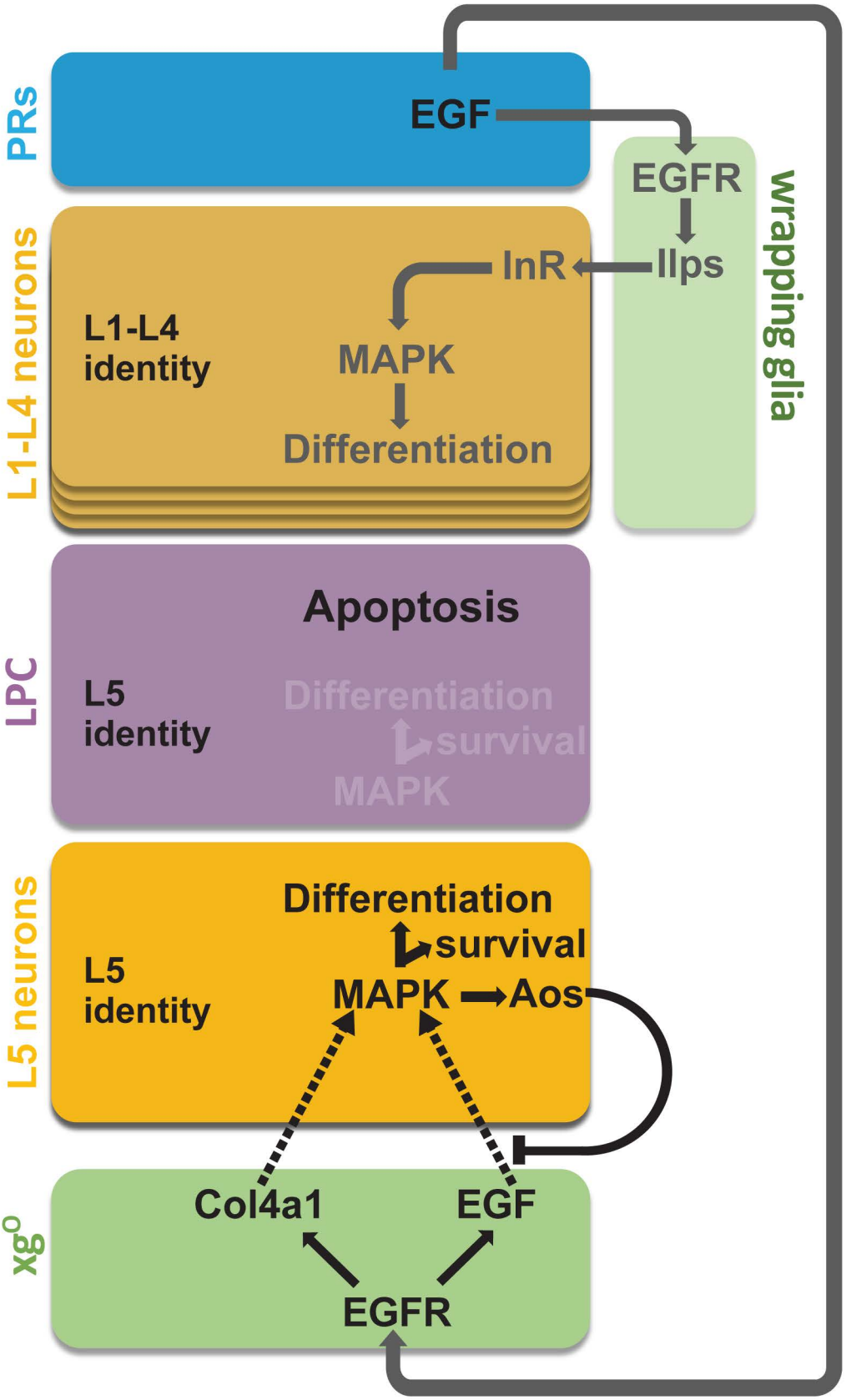
PRs
EGF
EGFR
Ilps
wrapping glia
L1-L4 neurons
InR
L1-L4
identity
MAPK
Differentiation
LPC
Apoptosis
L5
identity
Differentiation
survival
MAPK
L5 neurons
Differentiation
survival
L5
identity
MAPK
Aos
Col4a1
EGF
xg$^{O}$
EGFR